Trends in Analytical Chemistry 197 (2026) 118693

Contents lists available at ScienceDirect

Trends in Analytical Chemistry

journal homepage: www.elsevier.com/locate/trac

Exploiting the penetration depth of XRF and NIR radiation: from 2D to 3D spectral imaging

Zelan Li [a], Carolina Scagliarini [b], Alberto Mazzoleni [b], Sara Gariglio [c,d], Emilio Catelli [a], Cristina Malegori [c], Silvia Prati [a], Eugenio Alladio [b,*], Giorgia Sciutto [a,**], Paolo Oliveri [c,***]

[a] Department of Chemistry "Giacomo Ciamician", University of Bologna, Via Guaccimanni 42, 48121, Ravenna, Italy
[b] Department of Chemistry, University of Turin, Via Pietro Giuria 7, Torino, Italy
[c] Department of Pharmacy (DIFAR), University of Genova, Viale Cembrano 4, Genova, Italy
[d] Department of Chemistry and Industrial Chemistry (DCCI), University of Genova, Via Dodecaneso 31, Genova, Italy

ARTICLE INFO

Keywords:
X-ray fluorescence
Near-infrared
Spectroscopy
Penetration
Chemometrics

ABSTRACT

The present review examines the fundamental mechanisms governing the penetration of X-ray and near-infrared (NIR) radiation under sample surface – a feature that is often disregarded in analytical applications, especially in the spectral imaging implementations, which are usually considered as surface analytical techniques. The impact of material composition and geometry, scattering effects, as well as instrumental factors are thoroughly described and critically discussed. A particular focus is placed on data processing techniques, from first-principle equations to data-driven multivariate models, implemented to estimate/assess the extent of penetration. Applications in several areas, including food, forensic, material and cultural heritage sciences, are comprehensively reviewed. The potential for exploiting penetration of electromagnetic radiation is highlighted, paving the way for the development of 3D-resolved X-ray fluorescence (XRF) and NIR imaging approaches able to characterize multi-layer samples in a non-invasive way.

1. Introduction

The primary goal of an imaging technique is to capture and represent information about a surface or scene in a manner that can be analyzed, interpreted, and utilized for various applications [1]. When the focus shifts to spectral imaging, the essence lies in the simultaneous collection of spatial data (images) and spectral data, resulting in a full spectrum at every pixel of the image. A wide variety of instrumentation is currently available for such techniques, operating under different scanning modes: point-scan (also called whiskbroom), line-scan (pushbroom), and plane-scan [2]. These instruments implement sensing principles embracing the main spectroscopic techniques of analytical interest, including ultraviolet–visible (UV–Vis), fluorescence, near-infrared (NIR), mid-infrared (MIR), Raman, X-ray fluorescence (XRF), nuclear magnetic resonance (NMR), and mass spectrometry (MS), at both the microscopic and the macroscopic scale [2]. All the above methods can be catalogued under the general definition of hyperspectral imaging methods (HSI), particularly for their broad spectral coverage and the ability to analyze large or complex sample areas in a single experiment. HSI is generally considered a non-destructive analytical technique and, indeed, in many cases measurements are performed avoiding any physical contact to the sample at all, making it well-suited for sensitive or valuable materials.

However, these advantages come at the cost of generating massive datasets, which makes data mining and processing a major concern. In fact, the size of the data recorded may reach hundreds of MB, or even of GB, for a single spectral image. Data analysis can be performed at the pixel level, at the object level, or at the image level, depending on the characteristics of the data and, especially, on the analytical problem to be addressed [3]. Information embodied in spectral images has a high potential for the characterization of heterogeneous surfaces, providing the analyst with both a chemical mapping of key compounds and a determination of physical properties, such as reflectivity, texture, and roughness.

While research focuses on developing advanced data processing strategies to fully exploit the large volumes of HSI data, a related but

* Corresponding author.
** Corresponding author.
*** Corresponding author.
E-mail addresses: eugenio.alladio@unito.it (E. Alladio), giorgia.sciutto@unibo.it (G. Sciutto), paolo.oliveri@unige.it (P. Oliveri).

https://doi.org/10.1016/j.trac.2026.118693
Received 8 February 2025; Received in revised form 31 October 2025; Accepted 21 January 2026
Available online 23 January 2026

less-explored opportunity, especially for NIR spectroscopy, lies in leveraging the ability of radiation at certain wavelengths to penetrate below the surface. Traditionally, acquiring spectral imaging data through HSI involves capturing two spatial dimensions (x, y) along with a spectral dimension (λ). Nevertheless, the information of subsurface material composition may be inherently present but hidden within these datasets, since radiation at certain wavelengths possesses the capability to penetrate beneath the surface.

To move from purely surface-based imaging to a true volumetric imaging approach, one must rely on radiation capable of penetrating beneath the surface. Among the spectral regions used for analytical spectroscopy, NIR and X-ray have clearly demonstrated a substantial penetration ability due to absorption and scattering properties. X-rays penetrate thanks to the high energy of the used photons [4], while the NIR is particularly effective because its photons present energies that do not often match strong electronic transitions, thus leading to fewer absorption events [5]. Currently, due to the widespread use of imaging techniques, several instruments have been developed to perform imaging in NIR and X-ray regions, including point-scan based XRF imaging, and point, line scans based NIR imaging [6].

The joint application of XRF and NIR spectroscopies provides the analyst with a comprehensive sample characterization, merging complementary information both at the elemental and molecular levels, which can be exploited by application of suitable multiblock chemometric methods. Such a powerful integration is nowadays implemented by dedicated multiplatform instrumentation [7]. Extracting information from sample layers under the surface by analyzing data obtained with this type of instrumentation appears as an emerging analytical goal. For these reasons, the two spectroscopic techniques are discussed together in the present review paper.

Despite the advantages, the penetration potential depends critically on understanding the depth to which these radiations can travel. One of the main reasons why 3D volumetric imaging remains underexplored, especially in the NIR domain, is the challenge of determining the penetration depth. Nonetheless, several studies demonstrate that, with systematic approaches and advanced statistical analyses, it is possible to retrieve information from beneath the surface.

The phenomenon can be studied from the perspective of material science, optical physics and engineering, as well as from the viewpoint of chemistry, with all of these disciplines providing complementary information. The possibility of exploiting electromagnetic radiation penetration beyond sample surface for non-destructive volumetric analytical characterizations, is of considerable interest for many application fields. These range from biomedical diagnostics to forensic analysis, from cultural heritage conservation to food and pharmaceutical quality control.

Recent advancements in instrumentation, computational algorithms, and cross-disciplinary collaboration have made it more feasible than ever to capture and interpret volumetric spectral data. Nevertheless, the knowledge required to fully leverage NIR and X-ray penetration remains dispersed across multiple scientific domains, highlighting the need for a unified perspective. The aim of the present review is therefore twofold: first, to present the theoretical factors that modulate the penetration of NIR and XRF, which are the key parameters to describe the behaviors of radiation-matter interaction in these two regions; and second, for the first time, to consolidate the dispersed information into a coherent framework, seeking to advance the handling of challenges in acquiring, interpreting, and applying complex volumetric spectral imaging data.

Accordingly, the present review paper examines studies in which radiation penetration was critically investigated, with particular emphasis on the parameters governing penetration depth and on the potential to exploit this property for analytical purposes.

2. Fundamentals of XRF spectroscopy and penetration depth

XRF operates based on the interaction of X-ray photons with matter. The process begins when an incoming high-energy X-ray photon excites the atom in the irradiated material, causing the ejection of inner-shell electron through the photoelectric effect. As the atom stabilizes, electrons from higher energy levels transition to fill the vacancies, resulting in the emission of secondary, or fluorescent, X-rays [4,8,9]. This sequence of ionization followed by characteristic X-ray emission is referred to as the fluorescence effect, and forms the fundamental basis of XRF analysis. The energy of these emitted X-rays is characteristic of the elements present in the material, allowing for both qualitative identification and quantitative determination of their concentration.

XRF is capable of detecting a wide range of elements in various types of samples, including solids, liquids and powders, without requiring extensive preparation. As a non-invasive technique, XRF preserves the integrity of the sample, offers rapid results, and enables the detection of multiple elements simultaneously. These advantages make it particularly effective across diverse fields, such as cultural heritage, environmental science, archaeology, geology, and forensic analysis [10–13]. Moreover, the flexibility of XRF technology, from high-precision laboratory setups to compact portable instruments, supports for both controlled laboratory studies and real-time *in situ* analyses.

Based on the working principle of XRF, the X-ray penetration depth is primarily governed by the incident X-rays energy and the material composition under analysis. In contrast, the information depth, the depth from which fluorescent radiation can effectively escape the sample and be detected, is further influenced by several indirect factors, which modify the interaction between X-rays and materials, such as scattering and matrix effects.

To quantify the information depth more explicitly, a simplified mathematical expression (Eq. (1)) illustrates how multiple factors, such as energy, material composition and scattering, determine the depth range from which characteristic X-rays can be detected. When the primary X-ray beam interacts with the sample, the effective path length (d) can be expressed in simplified terms as:

$$d = x \cdot \sin \theta_{take-off} \quad \text{Eq. 1}$$

In Eq. (1), x represents the X-ray path length, which is influenced by the incident beam energy and the attenuation properties of the sample composition and density. The take-off angle $\theta_{take-off}$ is defined as the angle between the sample surface and the detector. Factors such as scattering and sample geometry influence this angle, thereby affecting the escape efficiency of the emitted fluorescence [4]. It should be noted that Eq. (1) represents a simplified model, assuming a homogeneous, flat sample and a uniform incident beam. In practice, both penetration depth and information depth in heterogeneous or multi-layered materials is far more complex, as variations in composition, density, and geometry lead to non-uniform attenuation paths.

Depth-related constraints directly impact the effectiveness of XRF in detecting elements and limits its capabilities in real applications. Understanding the penetration and information depth of XRF, as well as the factors affecting them, is fundamental for optimizing the applications across numerous scientific fields, particularly when the non-destructive analysis of multilayered samples is required.

For clarity, the four terms related to the "depth" used throughout the present review are defined below. "Penetration depth" refers to the physical depth to which the incident radiation can travel inside the material before its intensity is significantly reduced. This term only describes the path of the incoming radiation, not the outgoing signal. "Information depth" refers to the depth from which the detected signal actually originates. "Effective information depth" is a practical term for the maximum depth from which a signal can be successfully detected under the specific measurement conditions. "Depth resolution" indicates the ability to distinguish signals coming from different depths as separate contributions.

2.1. Variables affecting XRF penetration/information depth

Two primary factors — energy and material composition — work together with other variables to influence and determine how deeply X-rays penetrate, how they interact with the material, and how the resulting fluorescence is detected. Additional factors, such as matrix effect and scattering effect, can indirectly affect the information depth and therefore the effective information depth, by altering how efficiently fluorescence can escape and be detected from below the surface. These interrelated factors combine to shape the depth-resolved capabilities and overall quality of XRF measurements, affecting whether the analysis captures surface details or subsurface information.

2.1.1. Energy

The energy of the incident X-rays is one of the most important factors which directly influence penetration depth in XRF analysis. High-energy X-rays, typically in the range of 15–50 keV, have a greater capacity to penetrate deeper into materials compared to low-energy X-rays (below 10 keV). This difference arises because higher-energy X-rays have shorter wavelengths and higher frequencies, which reduce the probability of interaction with the outer electron shells of atoms. Instead, these high-energy photons primarily interact with the inner electron shells, such as the K-shell, thus passing through the sample with less attenuation. For instance, to effectively excite elements with high-energy fluorescence lines like zirconium (Zr, Kα ≈ 15.77 keV), the incident X-ray energy must be above its K-absorption edge of 18.0 keV. The high energy of both the incident and fluorescent X-rays facilitates the detection of signals from deeper layers of dense matrices. In contrast, exciting light elements such as silicon (Si, Kα ≈ 1.74 keV), which has a K-absorption edge at 1.84 keV, requires lower-energy incident X-rays. The low energy of the resulting fluorescence signal means it is easily absorbed by the matrix, limiting its analysis to the sample surface or very shallow depths [14].

2.1.2. Material composition

The composition of the material being analyzed is another core factor influencing the penetration depth in XRF analysis. As described by the Beer-Lambert law [4], the attenuation of X-rays through a material is governed by the mass attenuation coefficient (μ/ρ), where large mass attenuation coefficients lead to rapid attenuation and reduced penetration depth:

$$I \,/\, I_0 = e^{-(\mu/\rho)x} \qquad \text{Eq. 2}$$

This coefficient is primarily influenced by the energy of the X-rays and the atomic number (Z) of the material. While the coefficient itself is normalized with respect to density (ρ), the linear attenuation coefficient (μ) depends directly on the material density, affecting the overall attenuation and penetration depth. To obtain detailed attenuation data for a wide range of materials at various energies, the NIST XCOM Photon Cross Sections Database provides an authoritative resource [15].

As one of the primary factors influencing this coefficient, the atomic number (Z) has a direct impact on its ability to absorb X-rays through the photoelectric effect. Materials with a higher atomic number exhibit a greater probability for X-ray absorption. Consequently, high-Z materials, such as lead (Z = 82) or gold (Z = 79), significantly reduce X-ray penetration due to their efficient absorption.

In addition to atomic number, the density of the material, defined as mass per unit volume, is important for the X-ray attenuation. Indeed, denser materials contain more atoms per unit volume, thus increasing the probability of interactions between X-rays and the material, and reducing penetration depth. For example, tungsten (Z = 74, density = 19.25 g/cm^3) exhibits both a high atomic number and high density, resulting in very shallow penetration depths, while lighter and less dense materials, such as polymers, allow for much greater X-ray penetration. Polymers with densities around 0.9–1.4 g/cm^3 can allow X-rays to penetrate several millimeters, which is suitable for bulk sample analysis [4].

It is also important to recognize that atomic number and density, though related, are not always directly proportional. For example, while tungsten (Z = 74) has a lower atomic number than lead (Z = 82), it is actually denser (approximately 19.25 g/cm^3 versus 11.34 g/cm^3 for lead). According to NIST XCOM data, as an illustrative example at an energy of 20 keV, the approximate mass attenuation coefficients are about 65.73 cm^2/g for tungsten and about 86.37 cm^2/g for lead [15]. When multiplied by their respective densities, these mass attenuation coefficients result in linear attenuation coefficients of approximately 1265 cm^{-1} for tungsten and 979 cm^{-1} for lead. Therefore, at this specific energy, tungsten's higher μ value means that it attenuates X-rays more strongly than lead. It is critical to note, however, that this relationship is highly energy-dependent: a different incident energy would result in different attenuation coefficients and could reverse this outcome. This energy-dependence is especially pronounced in heterogeneous materials, where the presence of matrix absorption edges becomes the dominant factor controlling the information depth, a phenomenon discussed in detail in the following section.

2.1.3. Matrix effect

The matrix effect influences XRF analysis by altering the information depth of the fluorescence signal through variations in sample composition and density. This effect arises from interactions between the elements within the matrix, which can either absorb or enhance the fluorescence signals from the element of interest, potentially distorting the analysis. Matrix effects are generally categorized into absorption and enhancement effects [16].

Absorption effects are the most common and occur when non-target elements in the matrix absorb either the primary X-rays or, more significantly, the outgoing fluorescence X-rays from the target element. This phenomenon is governed by the presence of absorption edges in the matrix elements. The mass attenuation coefficient of a material exhibits sharp increases at its absorption edges (K, L, M shells). If the energy of a fluorescence line from a target element falls just above the absorption edge of a major element in the matrix, the signal will be severely attenuated. For example, consider the analysis of elements in an iron-rich matrix. A fluorescence signal from cobalt (Co, Kα at 6.92 keV), which has an energy just below iron's K-edge (7.11 keV), will be attenuated far less than the signal from manganese (Mn, Kα at 5.9 keV). This demonstrates how the presence of a single absorption edge can cause neighboring elements, like manganese and cobalt, to have dramatically different information depths within the exact same material. This non-linear effect is fundamental to understanding depth profiles and is a key consideration in the analysis of complex, multi-element samples like alloys, geological cores, and historical paintings.

Conversely, enhancement effects, or secondary fluorescence, occur when fluorescence from a high-Z element in the matrix has enough energy to excite a lower-Z target element, artificially increasing its signal and altering the perceived depth of analysis.

To address matrix effects, correction methods such as the Lachance-Traill algorithm and the fundamental parameter (FP) approach are commonly used [16]. The Lachance-Traill algorithm uses empirical coefficients to adjust for matrix interactions, while the FP approach relies on theoretical models to calculate X-ray interactions with the matrix. Other practical correction techniques include standard addition and internal standards, which are particularly useful when dealing with highly complex matrices that cannot be easily modeled [4].

2.1.4. Scattering effects

Scattering is a key factor in XRF analysis that indirectly influences the effective information depth by redirecting or attenuating X-rays as they interact with the material. This phenomenon occurs when X-rays interact with the atomic electrons in the material changing direction, potentially losing energy in the process. Two main types of scattering are

relevant to XRF: Compton scattering and Rayleigh scattering.

Compton scattering is more prevalent at higher X-ray energies. In this process, an incident X-ray photon collides with an electron, transferring part of its energy to the electron and altering its direction [17]. The resulting scattered photon has reduced energy and may no longer contribute effectively to the generation of the fluorescence signal. Compton scattering effectively limits the information depth because scattered X-rays are less likely to reach the detector or interact with deeper material layers. This type of scattering is particularly relevant in biological samples or other materials where the atomic number is relatively low [4].

Rayleigh scattering, on the other hand, is an elastic scattering process, meaning that the X-rays change direction without losing energy. This type of scattering is more prominent at lower X-ray energies and tends to occur more frequently in materials with high atomic numbers. High-Z materials like lead and gold exhibit greater Rayleigh scattering, further diminishing the depth at which X-rays can penetrate [4].

2.1.5. Geometric factors

The geometric factors discussed here include both the geometry of the instrument setup and the physical geometry of the sample. These factors influence information depth by affecting the path length, scattering, and detection efficiency.

The geometry of the XRF instrument setup, including the orientation of the tube, detector, and sample, significantly affects the actual penetration by altering path length, scattering, and detection efficiency. Several key aspects of geometry, such as the take-off angle, sample shape, and scattering angle, influence the actual penetration and accuracy of XRF analysis.

As mentioned, the take-off angle is critical as it defines the path length for the emitted fluorescence to escape the sample. This escape path length is inversely related to the sine of the take-off angle ($\sin \theta_{take-off}$). Therefore, a smaller take-off angle, for instance a more grazing exit, increases the path length which the fluorescence must travel through the material. This results in higher attenuation and a reduced effective information depth, making the analysis more surface sensitive. Conversely, a larger take-off angle (close to 90°) shortens the X-ray escape path, minimizing attenuation and allowing for the detection of signals for deeper layers. Optimizing the take-off angle is essential for balancing surface and subsurface sensitivity, depending on the analytical requirements.

The shape of the sample, particularly for irregular or non-flat surfaces like rough textures or curved forms, introduces variability in the X-ray path length, increasing the probability of scattering. These variations can complicate the estimation of information depth and reduce the consistency of the detected signal. In these cases, optimizing the angle of the X-ray beam and detector setup can help mitigate scattering effects and improve measurement accuracy.

The scattering angle describes the direction change of X-rays after interacting with the sample. In XRF analysis, when the scattering angle increases, the energy shift of the scattered X-rays due to Compton scattering becomes more pronounced, although the intensity of the scattered signal decreases. Controlling the scattering angle enables the minimization of the background noise and the improvement of the accuracy of the data, particularly when using geometries that involve backscatter detection.

In practice, different XRF configurations employ specific geometric setups to optimize analytical performances. For example, total X-Ray fluorescence (TXRF) uses a grazing incidence angle combined with a near 90° detection geometry relative to the incident beam, minimizing scattering and improving detection limits to the part-per-billion (ppb) range under controlled benchtop conditions [8]. In contrast, handheld XRF devices commonly use a triangular geometry (source-sample-detector) that increases coherent scattering while enhancing portability and making the instrument suitable for rapid on-site measurements [18].

2.1.6. Instrumentation and technique-specific factors

Different types of XRF instruments use varying energy levels and detection systems. As a result, both the physical penetration capabilities and the effective information depth of the detected fluorescence can vary. These factors collectively determine how effectively each system can probe beneath a sample surface, thus influencing its suitability for different analytical requirements and sample types.

Laboratory-based XRF systems generally include wavelength dispersive XRF (WDXRF), energy dispersive XRF (EDXRF), and synchrotron based XRF (SR-XRF). WDXRF and EDXRF both present tunable excitation energies, which affect how deep the X-rays penetrate, but the analytical trade-offs are different [8]. EDXRF is typically faster, making it ideal for rapid screening, but its lower spectral resolution can limit the precision of depth-related measurements [19]. WDXRF, on the other hand, offers better energy resolution, enabling more refined depth profiling and improved discrimination between signals originating at different depths [16]. In contrast, SR-XRF employs highly intense X-ray beams generated from a synchrotron source. While the fundamental penetration depth is still governed by the photon energy and the material, the extremely high photon flux of a synchrotron beam markedly improves the signal-to-noise ratio (SNR). This increases the effective information depth, making it possible to detect the very weak fluorescence signals that originate from deep within a sample: signals that would be lost in the noise of a conventional laboratory source. Furthermore, the ability to precisely tune the incident energy allows for selective excitation of elements and controlled, layer-by-layer analysis. These combined advantages make SR-XRF exceptionally powerful for examining the internal structures of complex, multilayered materials [19].

It is important to distinguish between physical penetration depth and effective information depth. The physical depth distribution from which fluorescence originates is governed by fundamental attenuation of both the incident and emitted photons, which depends on energy, geometry, and the material's absorption and scattering properties [4,8]. Increasing the incident flux (for example in synchrotron-based XRF) does not alter those attenuation coefficients and therefore does not increase the intrinsic penetration depth. Instead, higher flux improves the SNR and lowers the detection limit for weak fluorescence generated at depth. In practice, this extends the "effective" depth from which a useable analytical signal can be recovered, even though the underlying depth-weighting function of the radiation–matter interaction remains unchanged. This distinction is essential when comparing laboratory instruments, portable systems, and synchrotron setups.

Portable XRF (pXRF) is designed for on-site, field-based analysis. The energy levels in pXRF are moderate, usually optimized for surface and near-surface analysis. Due to the portability and power limitations, pXRF generally achieves penetration depths suitable for shallow subsurface analysis, effective for screening purposes in applications like environmental monitoring or archaeological surveys [18].

Another group of XRF techniques that specialize in depth-resolved analysis, designed to selectively target specific depths within a sample, offers enhanced spatial resolution and the ability to target surface and subsurface features. In this context, for instance, TXRF is designed for surface-level analysis using a grazing incidence angle. This geometry minimizes penetration depth, making it ideal for detecting trace elements with exceptional surface sensitivity, particularly in thin films or very small sample quantities [4,20]. Confocal XRF, on the other hand, offers the capability of depth profiling through a combination of focused excitation and detection optics. By aligning both the X-ray excitation and detection volumes to a precise focal point within the sample, confocal XRF can selectively measure fluorescence from different depths, thereby enabling the construction of a three-dimensional profile of the material [8]. Confocal XRF does not probe deeper, but instead provides depth discrimination through its use of focused excitation and detection optics. By defining a small, localized probe volume within the sample, it can selectively measure fluorescence from a specific layer.

While the maximum accessible depth is still fundamentally limited by X-ray energy and material composition (typically ranging from micrometers to a few millimeters), the unique strength of confocal XRF is its ability to construct a 3D elemental profile by scanning this focal point [21].

X-ray fluorescence computed tomography (XRF-CT) represents one of the most direct approaches for 3D volumetric analysis. Analogous to medical CT scanning, this technique involves irradiating a sample with a focused X-ray beam and measuring the resulting fluorescence as the sample is rotated and translated. Using tomographic reconstruction algorithms, a full 3D map of the elemental distribution within the sample's volume can be obtained [22]. XRF-CT is an unparalleled non-destructive tool for visualizing the internal structure, stratigraphy, and inclusions within complex samples. It has been applied in fields such as biomedical research [23,24], materials science [25,26], environmental geochemistry [27] for non-destructive investigation of complex, heterogeneous objects.

However, it is worth noting that XRF tomography yields three-dimensional elemental distribution maps, rather than from the acquisition of a continuous spectrum for each voxel. While 3D tomographic mapping is achievable with XRF, the resulting datasets reflect the presence of specific elements, as opposed to a spectral imaging measurement.

For analysis focused on the extreme near-surface (from nanometers to a few micrometers), grazing-incidence XRF (GI-XRF) and grazing-exit XRF (GE-XRF) are powerful laboratory and synchrotron techniques. In GI-XRF, the incident X-ray beam strikes the sample at a very shallow angle, at or below the critical angle for total external reflection. This confines the excitation to the top few nanometers of the surface, providing exceptional surface sensitivity. By varying the angle of incidence, depth profiling of the near-surface can be achieved. GE-XRF operates similarly but controls the angle of the detected fluorescence, allowing for depth-sensitive information to be obtained based on the escape path of the photons [28,29]. Both are essential techniques for characterizing thin films, layered nanostructures, and surface contamination [30–32].

The reader interested in the details of instrumentation described in the present paragraph is referred to Vanhoof et al. (2024) [22].

2.2. Applications related to penetration depth in XRF spectroscopy

XRF has been established as a versatile non-destructive technique across various research fields, resulting in more than 33,000 publications in the Scopus database, dating back to 1960s. The yearly number of publications has increased rapidly, particularly after 2000. Notably, the integration of XRF with imaging techniques appeared in the early 1990s and has shown a marked increase, with a sharper rise observed after 2010.

In contrast, when the search was restricted to XRF combined with depth-related terminology, the number of publications is much lower, highlighting its relatively limited focus compared to the broader use of XRF. A first pass using generic terms such as "penetration depth" returned only about 1590 publications. To minimize counting unrelated records, such as "penetration depth" in mechanical test or phrase like "in-depth review", a refined query was used to identify publications specifically focused on the analytical concepts of information depth, depth-resolved, or stratigraphy (see Supplementary Table S1 for the full query), resulting in a more relevant dataset of 834 publications (data retrieved on October 28th 2025).

This "depth-specific" sub-field shows clear growth in recent years, with a notable increase after 2015 (Fig. 1, bars). To evaluate whether this increase simply reflects the overall expansion of XRF publishing, the yearly counts were normalized to the total number of XRF publications in the same year. The resulting relative trend confirms that the "depth-specific" analysis is becoming a more visible research focus within the XRF community and not only a by-product of overall publication growth (Fig. 1, orange line and dotted line).

Within this trend, aside from publications focusing on the technique itself or its development, a significant portion has been dedicated to applications in specific fields, such as earth and planetary sciences,

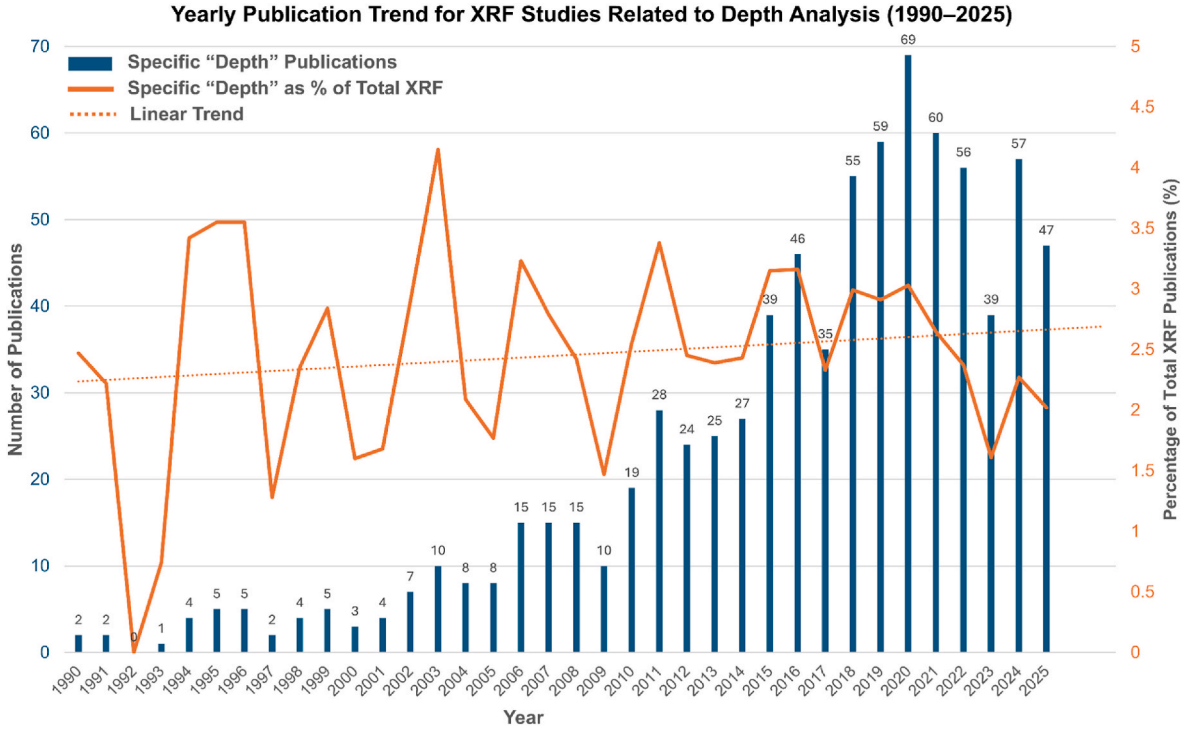

Fig. 1. Yearly publication trend for XRF studies related to depth analysis (1990–2025). The bars (left axis) represent the absolute number of publications retrieved using the specific "depth-resolved" query (see Supplementary Table S1). The line (right axis) represents these results as a normalized percentage of the total annual XRF publications, with its linear trendline shown (dotted line). Data were retrieved from the Scopus database on October 28th 2025.

cultural heritage, environmental science, and material science (Fig. 2). This emphasis may stem from the multilayered nature of samples in these fields, which require non-destructive, depth-sensitive techniques to effectively analyze their stratified structure and compositions.

The exact queries used for conducting searches in the Scopus database to analyze publication trends and subject areas are provided in the supplementary material (Supplementary Table S1).

Beyond the bibliometric trends, the literature reported a wide range of effective information depths and depth resolutions. At the nanometer scale, GI- and GE-XRF have been applied to thin films and nanostructures, achieving sub-nm to few-nm profiling [30,31,33]. At the micrometer scale, confocal μXRF has been characterized with instrumental depth resolutions of about 77 μm at 15.3 keV in a synchrotron setup [34], and 47 μm (Ca Kα) to 15 μm (Sr Kα) with absorption correction [35]. These instrumental values translate into practical layer separation in applications, such as the distinction of 5–10 μm prehistoric pigment layers from calcite supports [36]. At the millimeter scale, pXRF investigates bulk volumes in soils, plants, or hard tissues; for example, Sr detection has been confirmed through ~1.9 mm of bone [37]. Moreover, XRF-CT ranges across these scales by enabling 3D reconstructions, from tens of nanometers voxels, at synchrotron sources, to micrometer-scale mapping in geological and biological samples [38,39].

Taken together, these examples illustrate how depth sensitivity in XRF is not a fixed parameter but a technique- and matrix-dependent property, and this variability underpins the diverse applications reviewed in the subsequent sections.

Cultural heritage stands out as one of the prominent fields exploiting XRF penetration depth, particularly for examining layered structures in historical and archaeological artifacts.

Alfeld and de Viguerie's review provides a thorough examination of various XRF methodologies, with an emphasis on the role of penetration depth in distinguishing between layered compositions [10]. They compare scanning macro-XRF (MA-XRF) using mobile setups to synchrotron-based MA-XRF, highlighting how each approach contributes uniquely to depth-sensitive imaging. Moreover, Alfeld and de Viguerie discuss confocal XRF, noting its strength in providing localized depth profiles, which have allowed researchers to explore specific micro-layers without interference from surrounding materials. This has proven essential for analyzing micro-scale stratigraphy in historical artifacts.

Confocal micro-XRF and MA-XRF are the most commonly referenced techniques in studies on cultural heritage involving penetration depth. Confocal micro-XRF has been particularly valuable in cultural heritage for achieving depth-resolved, layer-by-layer analysis of materials. Kanngießer et al. applied confocal micro-XRF to study stratigraphy in painted ceramics and corroded metals, effectively differentiating micrometer-thick layers to reveal pigment sequences and degradation products specific to each layer [40]. Tapia et al. further demonstrated the use of confocal XRF depth profiling in prehistoric cave art, where it separated red iron-based pigments from calcitic substrates, improving the characterization of complex, multi-layered compositions on ancient surfaces [36]. MA-XRF, in contrast, is typically employed for broader surface mapping, with applications on large-scale artwork where layer thickness estimation is needed. Zito et al. demonstrated MA-XRF capability to estimate pigment layer thickness by analysing the attenuation of lead fluorescence lines (Pb Lα and Lβ), applying the Lambert-Beer law. Their study focused on Renaissance paintings, using thickness maps to reconstruct underlying pigment sequences, providing valuable insights into original compositions hidden by later modifications [41]. MA-XRF has also shown efficiency in various case studies, including Dal Fovo et al. examination of pigment layers in 16th-century artwork and Cavaleri et al. assessment of varnish and overpainting on a panel attributed to Raphael [42,43]. This method adaptability is further illustrated by Orsilli and Caglio, who used MA-XRF to investigate corrosion layers on ancient bronzes, connecting depth-related corrosion patterns to environmental exposure and preservation needs [44]. In some cases, multiple techniques are employed to enhance depth-resolved analysis. Dik et al., for instance, used synchrotron-based XRF to visualize a hidden portrait beneath Van Gogh "Patch of Grass", demonstrating how synchrotron XRF can access concealed paint layers with greater sensitivity

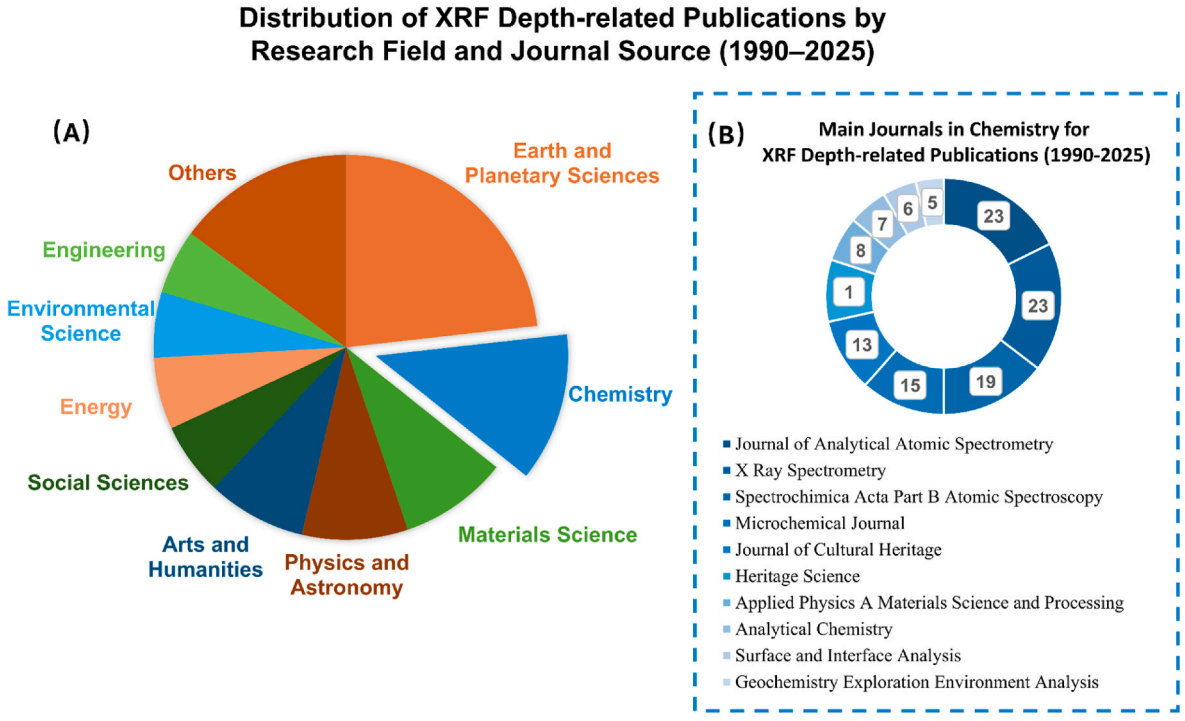

Fig. 2. Distribution of XRF depth-related publications by research field and journal source (1990–2025). (A) Distribution of publications across the top 10 research fields. (B) Journal distribution focusing exclusively on the subset of chemistry-related publications. Data were retrieved from the Scopus database on October 28th 2025.

and detail than conventional methods [45]. Similarly, a combined approach by Alfeld and Broekaert reviewed mobile XRF setups, emphasizing how mobile depth profiling methods, including both MA-XRF and confocal XRF, have expanded *in situ* capabilities for layered analysis in historical paintings [46].

Notably, GI-/GE-XRF approaches have been increasingly explored to non-invasively investigate in layered cultural heritage materials such as gilded metals, ceramics, and decorated surfaces. Nakano and Tsuji applied a combined confocal and GE-XRF setup to study Japanese *Tamamushi-nuri* lacquerware, demonstrating depth-sensitive characterization of multilayer structures [47]. More recently, Orsilli et al. employed grazing techniques at the Elettra synchrotron to examine Renaissance luster ceramics, revealing the presence of nanometric silver-rich layers despite the complexity of the glaze structure [48].

Penetration depth of XRF is also exploited in the environmental science, particularly for the assessment of soil and sediment contamination. In this field, pXRF is commonly used for in-field soil analysis due to its ease of deployment and non-destructive nature, but its limited penetration depth (~3.2 mm in soils) restricts its applicability for depth-resolved studies. Liang et al. (2018) demonstrated the use of pXRF to rapidly evaluate arsenic contamination in paddy soils, emphasizing the importance of sample geometry and positioning to optimize the limited penetration depth of pXRF [49]. By analyzing rice roots, which naturally accumulate arsenic in iron plaques, the study overcame the limitations of soil analysis by leveraging thinner, less dense organic structures that allowed sufficient X-ray penetration. While pXRF provided rapid surface-level contamination profiles, achieving reliable depth-specific measurements required careful calibration and validation against laboratory techniques, especially for elements which exhibit strong matrix effects, like arsenic. This approach highlights the relationship between penetration depth and sample characteristics in extending the applicability of pXRF to environmental assessments.

For more detailed depth profiling, particularly in environmental samples with stratified layers, XRF core scanning has proven its effectiveness. In Hennekam et al., XRF core scanning was applied to sediment cores to create high-resolution depth profiles of trace metals, including vanadium and molybdenum, within biogeochemical layers [50]. By scanning cores in sequential layers, this method enabled researchers to reconstruct historical contamination trends and correlated trace metal concentrations with periods of bottom-water anoxia and industrial activity.

Additionally, XRF penetration depth is also significant for analysing multi-layered biological materials. In this context, Rincheval et al. explored the penetration depth of pXRF in plant materials, finding that most detectable signals originated from the first 2–6 mm of the sample [51]. While primarily focused on biogeochemical mapping of contamination from mine tailings, this study highlights the critical role of sample density, thickness, and calibration in achieving accurate layer-specific analysis.

For more detailed 3D investigations of environmental and biological samples, XRF tomography provides access to the internal distribution of elements. In environmental toxicology, it has been used to investigate arsenic bioaccumulation in earthworms exposed to polluted soils, with XRF-CT confirming the localization of As within the coelomic cavity of intact organisms [52]. At the nanoscale, combined synchrotron nano-CT and nano-XRF tomography have revealed the 3D distribution of cobalt nanoparticle aggregates (~200 nm) within the nematode *C. elegans*, enabling visualization of their translocation into tissues and even into developing embryos, with voxel sizes down to 50 nm [38]. In plants, μXRF-CT has been applied to study cadmium toxicity in soybean roots, showing Cd sequestration in cortex vacuoles under sublethal exposure and deposition in cell walls and vascular tissues under lethal concentrations [27].

The penetration depth of XRF also provides value for the forensic analyses, helping the examination of multi-layered evidence in cases such as automotive paint and trace contaminants. Nakano et al. demonstrated how confocal XRF can isolate and analyze each stratum in multilayered paint fragments. By resolving the elemental composition of each coating layer, this technique aids in forensic discrimination, allowing analysts to compare paint samples in cases involving vehicle collisions and/or transferred paint evidence [53]. For larger forensic samples or when investigating residues across broad surfaces, MA-XRF offers a complementary approach. Langstraat et al. highlighted MA-XRF utility in imaging forensic evidence, such as layered biological residues or gunshot residues on fabrics [54]. This technique enables the scanning of large areas to reveal distribution patterns across surface and subsurface layers, which can be particularly useful in examining evidence without needing to alter the original sample.

Further applications of penetration depth in forensic investigations are explored by Knijnenberg et al., who described how macro-XRF can analyze concealed or layered forensic evidence [55]. For instance, MA-XRF has been used to detect gunshot residue patterns even beneath blood stains, leveraging X-ray penetration to access subsurface information. Similarly, biological residues such as Fe in blood and Zn in semen have been mapped on complex substrates, showing XRF capability to analyze overlapping or partially hidden traces. Additionally, MA-XRF has been applied to detect transferred cosmetic residues, such as lipstick or foundation, during violent interactions, by mapping elemental markers like Ti and Fe. This demonstrates the role of penetration depth in accessing subsurface information critical for forensic examinations.

The ability of XRF to probe beneath surfaces is crucial for characterizing advanced materials, where performance is often dictated by the composition and structure of buried layers or internal features. XRF-CT, for example, provides invaluable 3D chemical information for understanding material performance and degradation. The technique has been used for the *in situ* 3D chemical imaging of industrial core@shell catalysts, allowing researchers to observe the distribution of active metals deep within the particle during operation [25]. More recently, multimodal XRF-CT has been applied to study catalyst deactivation by mapping the internal pore network of technical dehydrogenation catalysts and distinguishing accessible from coke-blocked pores [39]. At the nanoscale, XRF tomography has enabled quantitative mapping of Cr and Fe distributions at grain boundaries to elucidate mechanisms of intergranular corrosion in stainless steel [26].

For probing thin films and buried interfaces at the nanometer scale, GI-XRF and GE-XRF are widely used for non-destructive depth profiling. GI-XRF combined with X-ray reflectometry (XRR) has been applied to transparent conducting oxide thin films, showing how the depth profile of Ga dopants correlates with optical and electrical performance [30]. GE-XRF has been successfully applied to characterize periodic nanostructures. A laboratory-based, scanning-free GE-XRF setup was used to determine the line height (58 nm) and layer thickness (2.3 nm) of titanium oxide and hafnium (HfO_2) nanostructures, achieving results that were remarkably close to those obtained at synchrotron facilities [56]. Another lab-based GE-XRF setup demonstrated the ability to retrieve the bilayer thickness gradient of a nickel-carbon multilayer sample with sub-nanometer resolution [31].

3. Fundamentals of NIR spectroscopy and penetration depth

NIR spectroscopy is a rapid, non-invasive, non-destructive, and label-free analytical technique widely applied across various fields, including medical diagnostics, food quality control, and forensic investigation [5]. Operating in the region of the electromagnetic spectrum between 780 and 2500 nm (12,820 to 4000 cm^{-1}), NIR spectroscopy relies on radiation absorption by molecular overtones and combination bands.

Unlike mid-infrared (MIR) spectroscopy, which is based on harmonic fundamentals of molecular vibrations, NIR spectroscopy is dominated by anharmonic effects, with inter-mode anharmonicity playing the most substantial role in the resulting band shapes and intensities. Molecular vibrations in NIR can involve both stretching and bending modes.

Stretching vibrations, occurring at higher frequencies, may be symmetric or asymmetric, while bending vibrations (scissoring, rocking, wagging, twisting) occur at lower frequencies. The bands most frequently observed in the NIR region stem from the first, second, or third overtones of fundamental C–H, N–H, S–H, and O–H stretches and their combination bands. This set of vibration types contributes to the characteristic complexity of NIR spectra, where overlapping bands are common, and multiple vibrational modes may coexist in a single spectrum. The application of chemometrics is essential to address the challenges of straightforward chemical interpretation arising from these broad, overlapping NIR bands [57].

One of the main advantages of NIR spectroscopy, still not properly explored, is the ability to penetrate into samples, depending mainly on factors like the materials composition, wavelength and instrumental configuration. This greater penetration is possible due to the relatively low absorptivity of NIR bands – typically 10–100 times weaker than fundamental MIR bands – which reduces signal saturation while slightly sacrificing sensitivity. Consequently, NIR can analyze bulk materials with minimal sample preparation, enhancing the applicability for in-depth heterogenous samples [58].

Understanding the mechanisms of NIR penetration and the factors influencing it is essential for optimizing its applications across diverse scientific domains. Tailoring these parameters in response to sample characteristics ensures that NIR spectroscopy can be effectively adapted to meet the specific analytical needs of fields ranging from medical diagnostics to food and environmental sciences.

3.1. Variables affecting NIR penetration depth

Absorption in the NIR range is driven by the molecular composition of the material, providing valuable spectroscopic information but also limiting penetration depth as the energy is absorbed and converted into vibrational energy.

Several factors, including material composition, scattering effects, geometry, and wavelength, significantly influence the depth of NIR penetration. Understanding these variables is crucial for optimizing NIR spectroscopy in various fields.

3.1.1. Material composition

Organic materials generally allow for greater penetration due to their molecular composition, rich in bonds which absorb NIR radiation at specific wavelengths [59]. In biological tissues, the penetration is influenced by scattering and absorption properties, with key absorbers such as water, lipids, and proteins playing a significant role [60]. Studies demonstrated that, in bone and cartilage tissues, the water content significantly affects NIR penetration, with higher water content reducing the depth at which NIR radiation can reliably characterize tissue composition [61,62]. In bones, the interaction of NIR radiation with water molecules leads to a limited penetration. In contrast, NIR penetration can be more effective in drier tissues or tissues with lower moisture content. In food materials, the behavior of NIR radiation is like the one observed in biological tissues, with moisture content influencing penetration depth, at different wavelengths [63]. This effect has been particularly noted in various food quality assessments, where NIR spectroscopy has been applied to evaluate compositional attributes such as moisture, protein, and fat content.

3.1.2. Scattering effects

Scattering plays a crucial role in the interaction mechanism between NIR radiation and samples. Thus, NIR ray deviates from its original path due to particles or structures within the material. The degree of scattering is influenced by the material physical features, including size, density, surface roughness, and the arrangement of their internal structures [64]. In biological tissues, scattering is predominantly caused by structures like collagen fibers, cellular membranes and other microstructures. The size of these structures relative to the wavelength of the NIR radiation determines whether scattering follows the principles of Mie or Rayleigh scattering [65]. Rayleigh scattering occurs when the scattering particles are much smaller than the NIR wavelength, resulting in isotropic scattering where the intensity is distributed evenly in all directions. This is typically observed in homogenous, low-density materials. On the other hand, Mie scattering becomes dominant when particle sizes are comparable to or larger than the wavelength of incident radiation. This leads to anisotropic scattering, where the intensity of the scattered beam is directional, with a forward bias. In highly heterogeneous materials, such as vegetable or animal tissues, Mie scattering not only redirects radiation but also causes energy loss, reducing the effective penetration depth. Internal microstructures can act as scattering centers, amplifying this effect. These scattering effects complicate the propagation of NIR rays and impact the accuracy of spectral data, particularly in complex and layered materials.

3.1.3. Geometry impact

As mentioned, the geometric impact may refer to both the geometry of the instrument setup and the physical geometry of the sample. Although also the structural geometry of samples under examination seems to play a role in the depth of NIR penetration, this aspect has been scarcely investigated until now. A study of mandarin fruits showed that physical properties, such as the thick outer skin and segmented internal structure, significantly impact NIR beam penetration. At a wavelength of 808 nm, the thick mandarin skin attenuates beam intensity significantly, while the core and internal segments cause perturbations [66]. This behavior can be attributed to internal scattering of the radiation within the fruit complex structure, where the segmented pulp and juice vesicles act as scattering centers, diffusing and redirecting the NIR beam in multiple directions. These perturbations arise from the multi-layered composition of the mandarin, including the thick skin, membranes, and juice vesicles, which create scattering interfaces. The differences in density and optical properties between these layers further disrupt the uniform propagation of radiation, leading to localized variations in intensity. In contrast, smoother, more homogeneous materials enhance uniform NIR penetration. A similar study on persimmon fruits used backscattering images to estimate absorption and scattering coefficients based on the skins thickness and wavelength, further highlighting the role of structural complexity in penetration [67]. Understanding how geometry and scattering affect NIR penetration is essential for optimizing the application of NIR spectroscopy in a wide range of materials. These factors highlight the importance of adjusting measurement techniques to the specific physical characteristics of the sample, ensuring more accurate and reliable results.

3.1.4. Wavelength

Wavelength plays a crucial role in determining penetration depth. In general, longer wavelengths in the NIR range undergo less scattering and therefore have the potential to probe deeper layers. However, this trend is strongly limited by absorption features of specific chromophores, most notably water. Around intense water bands, absorption can dominate over scattering reduction, sharply decreasing the effective information depth in hydrated and high moisture materials, such as muscle tissue or certain fruits. As a result, penetration depth in real samples is determined by the balance between wavelength-dependent scattering and wavelength-dependent absorption, rather than by wavelength alone. For example, in healthy cartilage, the penetration depth is approximately 5 mm in the 1110–1430 nm range and less than 1 mm in the 1960–2500 nm range [68]. In the food science, cutting an apple into slices of different thicknesses was a strategy deployed to assess the penetration of NIR radiation in apple tissue, up to 4 mm, in the 700–900 nm range, and up to 2–3 mm in the 900–1900 nm range [69]. Similarly, a NIR-HSI study (940–1650 nm) on powder milk achieved an optimal penetration at a sample depth of 2 mm [70]. Deeper layers, such as 4 mm and 5 mm, led to signal degradation due to increased scattering.

Several factors may influence the penetration depth at specific

wavelengths, including the samples thickness, the highly forward-scattering nature of samples as well as temperature, which affects molecular vibrations and beam penetration [71]. Thicker samples generally limit the maximum penetration depth, as the amount of radiation that reaches deeper layers diminishes with increasing sample thickness. Temperature can also alter the absorption and scattering characteristics of the material in a wavelength-dependent manner, which further impacts penetration. It is important to note that these factors influence penetration depth differently depending on the wavelength: at shorter wavelengths, scattering tends to be more pronounced, limiting penetration while, at longer wavelengths, scattering effects are reduced, allowing for deeper penetration. This outcome highlights the importance of selecting the appropriate wavelength based also on the target tissue or material being under study, as different wavelengths interact uniquely with the materials composition and structure.

3.1.5. Other factors

The optical properties of a material, such as its refractive index and anisotropy, also affect how NIR radiation propagates. Anisotropic materials with complex internal structures may scatter radiation more, thereby reducing the effective information depth. The intensity of the NIR source and its coherence also influence effective information depth, with higher-intensity sources capable of recovering useable signals from deeper regions by overcoming absorption losses more effectively [72].

Understanding and controlling all these variables is critical for optimizing the performance of NIR spectroscopy across different scientific and practical applications. By carefully considering factors such as material composition, scattering effects, and wavelength, researchers can tailor NIR spectroscopy to specific needs, improving its accuracy and depth of penetration in diverse materials and tissues.

3.1.6. Instrumentation and technique-specific factors

Precise and reliable analytical techniques are essential for understanding NIR penetration within various materials and tissues. These techniques cover applications from medical imaging and diagnostics to material analysis and food science.

Given the specific analytical requirements, the possibility of varying instrumental configurations and analytical parameters have been investigated particularly in the clinical field.

Typically, in a NIR measurement, radiation is delivered to and collected from the sample through optical fibers (optodes) or other simple optical systems (*e.g.*, relay lenses), which simplify the instrumentation. Recent advancements in NIR technology, particularly in functional NIR spectroscopy (fNIRS), have further expanded its applications. fNIRS enables the mapping of brain activity by measuring changes in blood oxygenation, offering a non-invasive alternative to functional magnetic resonance imaging (fMRI) for specific applications [73,74]. By detecting variations in the concentrations of oxygenated (HbO_2) and deoxygenated (HbR) hemoglobin, fNIRS monitors functional activation in specific cortical regions during tasks or stimuli. fNIRS systems typically employ arrays of optical fibers configured to measure multiple spatial locations simultaneously, enabling detailed and localized mapping of cortical activity. These optical fiber-based systems allow NIR radiation to be delivered deep in hard-to-reach areas like the whole neonatal head in clinical studies, facilitating non-invasive monitoring. Using a semiconductor laser at various NIR wavelengths and positioning it at different locations on the head has achieved penetration depths between 6.3 and 8.5 mm [75].

Optical coherence tomography (OCT) exploits NIR radiation to generate high-resolution cross-sectional images. OCT provides detailed images with micrometer-scale resolution by measuring backscattered NIR time delay and intensity [76]. OCT is particularly effective for imaging superficial tissues, such as skin and retinal layers, but has also found applications in dermatology, cardiovascular research, and cancer diagnostics. Typically, OCT achieves a penetration depth of 1–2 mm, making it ideal for imaging superficial tissue layers. However, its depth is limited compared to other techniques due to the scattering and absorption properties of tissues [77]. The penetration of NIR radiation also offers OCT significant potential for cultural heritage studies, especially for transparent and semi-transparent materials including varnishes, glazes, and paint layers [78].

Diffuse reflectance spectroscopy (DRS) is valuable for assessing NIR penetration in highly scattering samples like biological tissues or powdered materials. The method relies on measuring the NIR beam diffusely reflected from a sample after multiple scattering events, providing information about both surface and subsurface layers. DRS has been used to demonstrate that optimizing sample size and thickness is critical for understanding how deeply NIR radiation penetrates into a material. The effective sample size – the portion of the sample contributing most significantly to the reflected signal – depends on the material scattering and absorption properties, as well as the wavelength. Ensuring the appropriate sample dimensions allows the measurements to accurately capture information from the target layers while minimizing interference from excessive scattering or absorption. This optimization is essential for reliably determining the effective information depth of NIR radiation in various materials [79]. An application in pharmaceutical analysis illustrates that combining DRS with multivariate analysis allows for detecting counterfeit drugs by evaluating the depth and distribution of radiation within solid dosage forms [80].

NIR spectral imaging combines spatial and spectral data acquisition, allowing for a comprehensive analysis of a sample compositional and structural properties. Unlike point-based methods, spectral imaging employs various acquisition modes, each suited to specific applications. In point-scanning mode, spectra are sequentially collected from individual points across the sample, providing high detail but requiring longer acquisition times. Line-scanning (or pushbroom) approach records spectral information along a line, progressively constructing a complete image and offering a balance between resolution and speed. Finally, plane-scanning (or snapshot) mode acquires the entire spatial and spectral information of a sample in a single acquisition, making it ideal for dynamic or rapidly changing samples. NIR spectral imaging enables the non-destructive characterization of subsurface layers and heterogeneous samples, providing high-resolution spatial and compositional information [81].

Each of the techniques has its strengths and limitations. fNIRS is widely used for quantitative measurements and non-invasive monitoring but has limited resolution in deeper tissues. OCT and DRS, on the other hand, offer high-resolution imaging but may have a limited penetration depth compared to single-point spectroscopic methods. Spectral imaging techniques provide a powerful combination of spatial and spectral data, enabling detailed analysis of heterogeneous samples. However, factors like scattering, absorption, and sample geometry must be carefully considered to optimize performance. The choice of technique often depends on specific application, the desired resolution, and the required depth of penetration.

3.2. Applications related to penetration depth in NIR spectroscopy

NIR spectroscopy is widely used for non-invasive analysis in various fields ranging from materials science, and cultural heritage to biomedical sensing, pharmaceuticals, food quality control and process monitoring. A broad Scopus search combing NIR with spectroscopic terminology returns more than 110,000 publications, dating back to 1940s (see Supplementary Table S2 for full queries). The yearly number of publications has grown significantly from the 1990s, driven by advances in instrumentation and expansion of applications.

To specifically investigate the focus on penetration depth related analysis, a refined query with syntax, as for XRF, was implemented to identify publications explicitly referring to concepts such as information depth, depth profiling, or stratigraphy (Table S2 for full queries). This more precise search returned about 800 publications mainly after 1990. Although these publications represent only a small fraction of the overall

NIR literatures, but the absolute number of publications has increased markedly over the last decade (Fig. 3, bars). When these counts are normalized to the total number of NIR spectroscopy publications per year, the relative proportion also shows an upward trend over time (Fig. 3, orange line and dotted line), clearly reflecting the growing attention.

The distribution of these depth-related NIR publications across different research fields and journal sources is shown in Fig. 4. The subject areas are highly diverse, with engineering, chemistry, biochemistry, and physics representing the major shares. This highlights the broad applicability of the technique, from fundamental physics to applied life sciences. Specified to the chemistry field, unlike the XRF researches which were concentrated in highly specialized spectroscopy journals, the NIR researches appear more in general interest journals, reflecting the broad interest to the wider scientific community. To illustrate the practical impact, the following sections will explore key applications and case studies.

It is worth noting that, in the following context, the reported "depth" values correspond to the effective information depth of the method, for instance, the depth from which a diagnostically useable signal can be retrieved under the given optical power, acquisition geometry, and SNR constraints, rather than the absolute physical propagation limit of NIR radiation.

In clinical studies, NIR spectroscopy has been extensively used for imaging and diagnostic purposes, with one of its primary applications being brain tissue analysis. Early studies demonstrated that NIR penetration depth in human brain tissues at 1060 nm is significantly greater in new-born individuals than in adults. Svaasand and Ellingsen (1983) developed a model with consideration given to factors of beam distribution within the tissue based on scattering and absorption characteristics, revealing that in adults, the penetration depth reached approximately 3.5 mm, while in new-born individuals, it was 2–3 times greater [82]. This difference is likely due to the degree of myelination and water content between neonatal and adult brain tissues. Another application in the medical field consists of the measurement of brain oxygenation and activity through functional near-infrared spectroscopy (fNIRS). This non-invasive technique provides real-time monitoring of hemoglobin concentrations and oxygenation levels in the brain. Recent advancements have significantly improved fNIRS resolution and signal quality, allowing it to be applied in clinical diagnostics and neuropsychological research. Haeussinger et al. (2011) studied the penetration depth of NIR radiation in the brain, showing that it typically varies between 2 and 3 cm, with most of the energy being absorbed by the superficial tissues, such as the scalp and skull. Approximately 96 % of the absorbed radiation remains in these tissues, with only 3 % reaching the grey matter, highlighting the limitations of fNIRS for deeper brain structures [83]. A specific method, Time-Resolved Spectroscopy (TRS), measures the time of flight of photons as they travel from a sending optode to a receiving optode. This approach provides detailed information about the propagation of NIR radiation through brain tissue. Perrey et al. (2008) showed that NIR radiation (in the 650–950 nm range) travels in a shallow arc within brain tissue, with a penetration depth of approximately half the source-detector separation distance, typically 2–3 cm [84]. This depth allows for sufficient analysis of cortical brain regions, providing clinicians with critical insights into brain oxygenation and blood flow. TRS has been particularly useful in assessing regional brain activity in tasks involving motor and cognitive functions, offering a dynamic and quantitative evaluation of cerebral hemodynamic. Another promising area of research is the development of non-invasive glucose monitoring devices for diabetic patients. NIR spectroscopy, particularly around 1600 nm and in the first overtone region between 1500 and 1850 nm, has been explored for its potential to measure glucose concentrations under the skin by targeting glucose-specific absorption bands. However, one of the significant challenges in non-invasive glucose monitoring using NIR spectroscopy is the shallow penetration depth (typically a few millimeters), largely due to the high-water content in skin tissues. This causes difficulties in distinguishing the glucose signal from the background signals of other

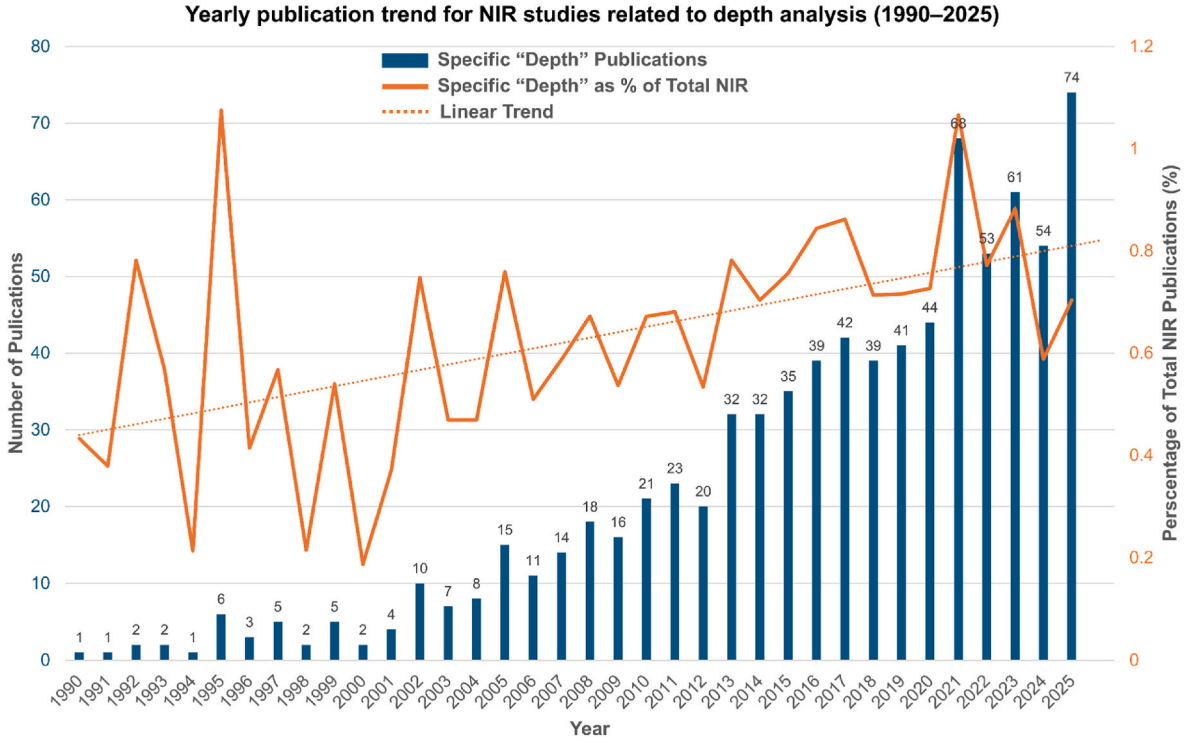

Fig. 3. Yearly publication trend for NIR studies related to depth analysis (1990–2025). The bars (left axis) represent the absolute number of publications retrieved using the specific "depth-resolved" query (see Supplementary Table S2). The line (right axis) represents these results as a normalized percentage of the total annual NIR publications, with its linear trendline shown (dotted line). Data were retrieved from the Scopus database on October 28th 2025.

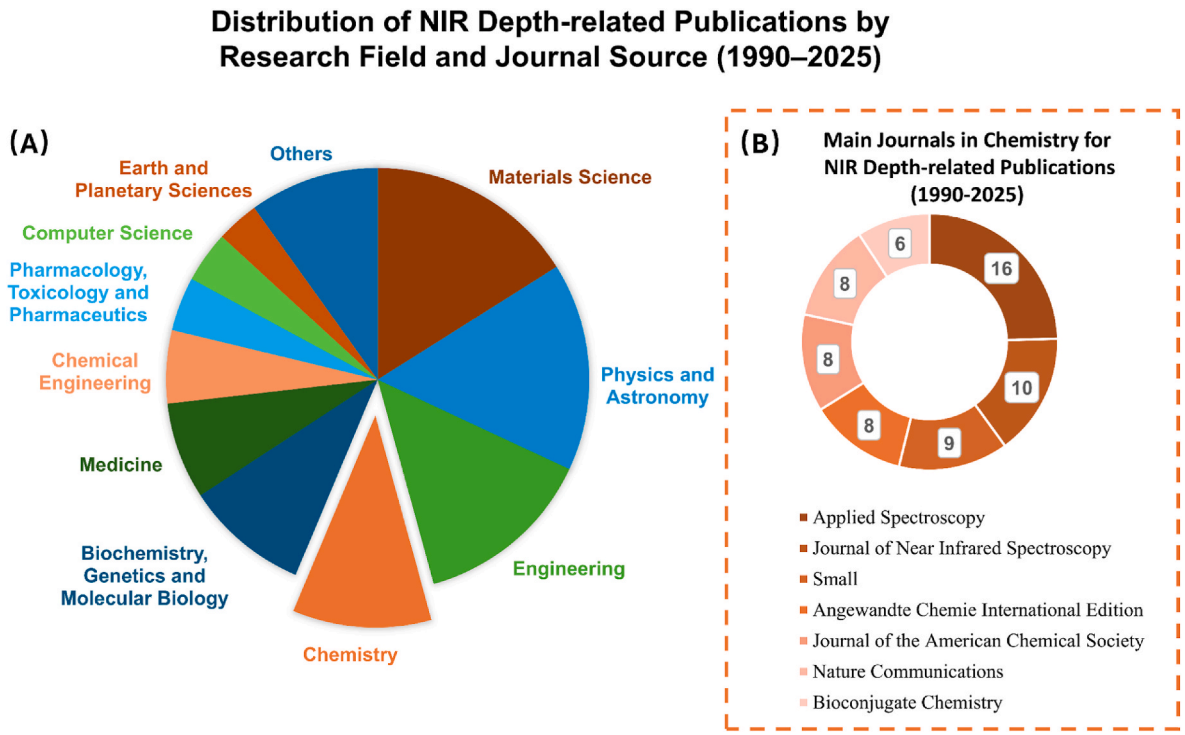

Fig. 4. Distribution of NIR depth-related publications by research field and journal source (1990–2025). (A) Distribution of publications across the top 10 research fields. (B) Journal distribution focusing exclusively on the subset of chemistry-related publications. Data were retrieved from the Scopus database on October 28th 2025.

chromophores, such as water, hemoglobin, and lipids [85]. This limitation has prompted ongoing advances in signal processing and sensor technology to enhance the accuracy and reliability of these measurements. Beyond brain tissues, NIR spectroscopy has also been successfully applied to assess other biological tissues, including cartilage. Padalkar and Pleshko (2015) demonstrated wavelength-dependent penetration depth in cartilage, reaching up to 5 mm between 1110 and 1430 nm, approximately 3 mm between 1430 and 1960 nm, and 1–2 mm in the 1960–2500 nm range [68]. This variability underscores how NIR penetration is influenced not only by wavelength but also by the thickness and structural properties of the tissue. The study further highlighted that increasing sample thickness alters the mode of data collection from transflectance to diffuse reflectance, demonstrating that NIR radiation interacts differently with various tissue zones (superficial, middle, and deep layers). This highlights the importance of tailoring NIR parameters to the specific tissue under investigation.

In pharmaceutical applications, NIR spectroscopy plays a pivotal role in quality control, particularly for assessing the homogeneity of excipients and active pharmaceutical ingredients (APIs) within tablets and for evaluating the uniformity of coatings and blends. Clarke et al. (2002) demonstrated that NIR reflectance microscopy can measure under-surface information in pharmaceutical materials by modeling them with cellulose-based samples. The study highlights that the penetration depth is highly dependent on wavelength, ranging from approximately 109 μm at longer wavelengths (2500 nm) to around 777 μm at shorter wavelengths (1100 nm), with a typical depth of 200 μm observed at 1675 nm [86]. Additional research on pharmaceutical powders has highlighted the effectiveness of NIR spectroscopy for quality analysis in compacted formulations. Mauritz et al. (2010) showed that Optical Coherence Tomography (OCT), when paired with NIR spectroscopy, can achieve high-resolution imaging of tablet coatings. In their study, two different wavelengths – 930 nm and 1325 nm – were evaluated, both achieving a penetration depth of approximately 0.5 mm. This application underscores NIR capacity for in-depth analysis of bulk and layered materials, facilitating non-destructive quality control that supports uniformity, efficacy, and safety in pharmaceutical products [87]. This capability enables detailed, non-destructive visualization of layer thickness and uniformity in pharmaceutical tablets, providing essential insights into the structural integrity of coatings and ensuring quality control during manufacturing. A comprehensive study by Yang et al. (2017) evaluated the performance of NIR across the 1200–2200 nm spectral range in solid pharmaceutical tablets using an acousto-optic tunable filter (AOTF) NIR spectrometer. Their findings indicated that NIR can penetrate depths of up to 2 mm in certain formulations, emphasizing the technique applicability in assessing blend uniformity and active ingredient distribution. The study underscores the significance of wavelength selection and material properties in determining the effective penetration depth, allowing for improved monitoring of tablet composition and quality [88].

In forensic science, NIR spectroscopy has proven effective for examining biological and chemical traces. In bloodstain analysis, NIR spectroscopy has been applied to evaluate the aging process of bloodstains, detecting spectral changes in hemoglobin as blood ages on different substrates like gauze and glass. The penetration depth in these cases varies with the substrate, but no uniform penetration depth is mentioned across studies. However, evidence suggests that NIR can analyze surface layers and detect moisture content and blood degradation up to a few millimeters deep [89]. In fiber and textile analysis, NIR spectroscopy has been used to detect residues and differentiate fibers in forensic cases. For instance, studies have used NIR to identify chemical residues and even gunshot residue (GSR) on fabrics. One study demonstrated the use of NIR hyperspectral imaging (NIR-HSI) to identify GSR from non-toxic ammunition (NTA) containing luminescent markers. This method provided a non-destructive, fast, and surface-level analysis of GSR, with a success rate of over 72 % in correctly identifying GSR samples based on their chemical signatures. The study noted that NIR penetration was sufficient to detect surface-level residues and differentiate gunshot particles even with small samples, making it highly applicable to forensic fiber analysis. However, the characterization is typically limited to surface detection rather than deep penetration into

the material [90]. These findings highlight that, while NIR is valuable for surface detection and identifying biological fluids and fibers, the exact penetration depth in forensic materials is typically limited to a few millimeters, influenced by the material absorption and scattering properties.

Another field where the penetration characteristics of NIR radiation have garnered significant attention is cultural heritage, as it often involves the analysis of multilayered samples to uncover stratigraphic and compositional details. Longoni et al. (2022) explored the application of FT-NIR spectroscopy in the study of binders and multilayered structures in Renaissance paintings [91]. Using NIR radiation in the range of 7500–4000 cm^{-1}, their study highlighted the deeper penetration capability of NIR compared to MIR radiation. This allowed for the characterization of inner layers, including preparatory layer, even in complex stratigraphy. Although no exact penetration depth was directly measured, the study provided an indirect estimation of penetration through cross-sectional analysis, suggesting a depth of approximately 60–100 μm based on the observed spectral contributions of the layers [91].

For cultural heritage studies, another growing area of interest is the integration of NIR into HSI systems, which combine spectral and spatial information to investigate artworks non-invasively. By knowing the capability of NIR imaging in visualizing underdrawings and pentimenti beneath painted surfaces, Cucci et al. (2016) applied HSI in the NIR range (750–2500 nm) for analyzing old master paintings [92]. The study showcased NIR reflectance imaging as a powerful tool for extracting stratigraphic information indirectly through spectral analysis. Similarly, Catelli et al. (2023) presented a novel HSI system that integrates VNIR (400–1100 nm) and SWIR (1100–2500 nm) with XRF, combining molecular and elemental mapping with advanced multivariate and multiblock data processing methods to comprehensively analyze stratigraphic structures [93].

NIR spectroscopy has gained widespread use in the food industry for quality control and safety monitoring, especially in evaluating moisture content, protein levels, and fat in various food products. A detailed study was conducted on the penetration of NIR radiation in watermelon. Using a NIR system in interactance mode at 761–1081 nm, penetration depths ranged from 9 to 11 mm in intact watermelons and up to 11 mm in the red flesh of cut fruit [94]. These findings highlight how the penetration depth is strongly influenced by factors such as the thickness of the rind and the distance between the beam source and the sample. Further research by Greensill and Walsh (2000) assessed the internal attributes of intact rock melon fruit using a remote acceptance probe combined with a non-contact partial transmittance illumination configuration, optimized for the equatorial region of the fruit. This system achieved up to 15 mm below the fruit surface, providing sufficient data for assessing the soluble solid content (SSC) near the fruit equatorial region [95]. Despite the exponential decrease in signal strength with depth, NIR spectroscopy was effective for non-invasive assessment, even with non-contact configurations, demonstrating its potential in fruit sorting and quality assessment systems. Hyperspectral NIR imaging was used to evaluate penetration depths of up to 1.8 mm in powdered food products such as wheat flour. This depth was determined by acquiring hyperspectral images of varying wheat flour thicknesses (0.5–3.5 mm) in a PLA holder, applying PLS regression to quantify PLA spectral signatures, and using Kubelka-Munk theory to define penetration depth where reflectance stabilizes. The study demonstrated that wavelength, material properties, sample thickness, and sensor dynamic range significantly influence how NIR beam propagates through powdered samples [96]. In addition to these findings, further research has shown that moisture content is crucial in determining NIR penetration in various food products. Using a spectroradiometer system (700–2500 nm), a study on potato tissue measured the spectral hemispherical reflectance and transmittance on heat-treated potato tissue at different moisture levels and thicknesses [97]. The results indicated that higher moisture content reduces NIR penetration due to increased reflectance, thereby decreasing the fraction of incident energy absorbed by the material. For raw potato tissue, the penetration depth was approximately 1 mm, compared to 2.4 mm reported for ham in previous studies [98].

4. Data processing

The eldest studies concerning the assessment and modeling of penetration of NIR radiation, ranging from the 1980s to the first decade of the XXI century, mainly focused on physical aspects of spectral diffusion throughout different matters. To address this aim, besides a visual evaluation of spectral profiles, the underlying phenomena were typically modeled by fitting first-principle equations [79,82], which included least-squares fitting of modified forms of Lambert's law [75] and non-linear exponential functions [69,97]. Some studies combined model fitting with Montecarlo simulations of penetration levels [66], also exploring the effect of influent factors, such as the incident angle and the different wavelengths selected [70]. For example, Monte Carlo simulations were used to predict mean penetration depths in a two-layer tissue-mimicking phantom. By adjusting the fiber angle, the penetration depth into the intralipid layer can be controlled, achieving 125 μm penetration at 1459 nm with a 60-degree fiber angle, while minor penetration was observed in the epoxy phantom at wavelengths of 1187 nm and 1697 nm [99]. More recent studies, starting from 2010s, involved multivariate processing of spectral signals. Most of these works also explored the effect of signal pre-processing, testing several mathematical transforms typically used in the chemometric field for analysis of NIR spectra, including the standard normal variate (SNV) transform [70,71,94], Savitzky-Golay smoothing and derivatives [68,70,71,96], and multiplicative scatter correction (MSC) plus its extended version (EMSC) [70,71]. Some of these studies focused on the differential penetration extent as a function of the specific wavelength interval, using chemometric strategies such as interval split [68] and variable selection, performed by uninformative variable elimination (UVE) [71]. Multivariate data processing strategies applied included both exploratory unsupervised methods, such as principal component analysis (PCA) and cluster analysis (CA) [71], and supervised modeling. Concerning this latter branch, models were built both at the qualitative level, by means of classification methods – partial least squares discriminant analysis (PLS-DA) and support vector machines (SVM) [70,71] – and at the quantitative level, applying regression models – from linear partial least squares regression (PLSR) to non-linear artificial neural networks (ANN) [71]. The requirement for non-linear models can be justified by the complexity of the phenomena under investigation, which typically exhibit non-linear behaviors. The latest studies in this field explore the potential of chemometric signal unmixing strategies, such as multivariate curve resolution alternating least squares (MCR-ALS), to mathematically resolve the spectral contribution of chemical compounds constituting the different layers of samples [94].

Concerning the processing of XRF spectra, first-principle equation fitting is the widespread approach [100]. In particular, most of the studies applied equations derived from the theory of confocal measurements [53,101].

In some cases, Montecarlo simulations complemented the data processing strategy [102]. Multivariate data modeling of X-ray penetration extent is definitely less represented, if compared to what discussed for NIR spectroscopy.

5. Conclusions and perspectives

Ability of NIR and X-ray radiation to penetrate different materials opens new frontiers in spectroscopy and spectral imaging, enabling the non-invasive characterization of complex and heterogeneous multilayer samples.

While in-depth 3D mapping has been widely implemented in other spectral imaging fields, such as nuclear magnetic resonance (NMR), its application, especially within vibrational spectroscopies, remains

largely unexplored. To fill this gap, a key role will be played by the development of dedicated chemometric strategies.

In more detail, future work has to be addressed to further investigate on the instrumental factors that modulate the penetration and information depth of NIR and X-ray radiation, through multivariate design of experiments and response surface methodologies. This will lead to the possibility of acquiring multi-frame spectral images, while varying the levels of key instrumental factors, to record spectral information from deep sample layers in a differential sequence.

To process such complex data, the possibilities offered by data-driven machine learning in chemometrics have to be explored, with a particular focus on signal deconvolution and curve resolution methods.

Extraction and modeling of informative spectral features coming from undersurface sample layers will significantly enhance the analytical power of NIR and XRF spectral imaging techniques, making them the first-choice analytical platform in several application fields.

CRediT authorship contribution statement

Zelan Li: Writing – original draft, Visualization, Investigation, Data curation. **Carolina Scagliarini:** Writing – original draft, Visualization, Investigation, Data curation. **Alberto Mazzoleni:** Writing – original draft, Visualization, Investigation, Data curation. **Sara Gariglio:** Writing – review & editing, Investigation, Data curation. **Emilio Catelli:** Writing – original draft, Investigation, Data curation. **Cristina Malegori:** Writing – review & editing, Methodology. **Silvia Prati:** Writing – review & editing. **Eugenio Alladio:** Writing – review & editing, Methodology, Conceptualization. **Giorgia Sciutto:** Writing – review & editing, Methodology, Conceptualization. **Paolo Oliveri:** Writing – review & editing, Supervision, Resources, Project administration, Methodology, Funding acquisition, Conceptualization.

Declaration of competing interest

The authors declare the following financial interests/personal relationships which may be considered as potential competing interests: Financial support provided by the Italian Ministry for University and Research (MUR) is reported.

Acknowledgement

Financial support provided by the Italian Ministry of Universities and Research – MUR (Research Project PRIN 2022 n. 20223WBTH8, CUP: D53D23008950006; Research Project PRIN 2022 PNRR n. P20227N5YZ, CUP: J53D23014500001, D53D23016770001) is gratefully acknowledged.

Appendix A. Supplementary data

Supplementary data to this article can be found online at https://doi.org/10.1016/j.trac.2026.118693.

Data availability

No data was used for the research described in the article.

References

[1] J.M. Amigo, H. Babamoradi, S. Elcoroaristizabal, Hyperspectral image analysis. A tutorial, Anal. Chim. Acta 896 (2015) 34–51, https://doi.org/10.1016/j.aca.2015.09.030.
[2] N.C. Basantia, L.M.L. Nollet, M. Kamruzzaman (Eds.), Hyperspectral Imaging Analysis and Applications for Food Quality, CRC Press, January, 2018.
[3] C. Malegori, P. Oliveri, Principal component analysis, in: Hyperspectral Imaging Analysis and Applications for Food Quality, CRC Press, 2018, pp. 85–107.
[4] R. Jenkins, X-Ray Fluorescence Spectroscopy, Wiley PP, New York ; Chichester, 1988.
[5] Y. Ozaki, Near-infrared spectroscopy—its versatility in analytical chemistry, Anal. Sci. 28 (6) (2012) 545–563, https://doi.org/10.2116/analsci.28.545.
[6] P. Geladi, Are pixels sample cells? Hyperspectral diffuse near infrared imaging experiments with pinholes, J. Near Infrared Spectrosc. 16 (3) (2008) 357–363, https://doi.org/10.1255/jnirs.799.
[7] M. Occhipinti, et al., IRIS : a novel integrated instrument for co-registered MA-XRF mapping and VNIR-SWIR hyperspectral imaging, X Ray Spectrom. 53 (6) (Nov. 2024) 520–530, https://doi.org/10.1002/xrs.3405.
[8] B. Beckhoff, h.B. Kanngießer, N. Langhoff, R. Wedell, H. Wolff (Eds.), Handbook of Practical X-Ray Fluorescence Analysis, Springer, Berlin Heidelberg PP - Berlin, Heidelberg, 2006.
[9] B.L. Drake, B.L. MacDonald (Eds.), Advances in Portable X-ray Fluorescence Spectrometry: Instrumentation, Application and Interpretation, Royal Society of Chemistry, 2022.
[10] M. Alfeld, L. de Viguerie, Recent developments in spectroscopic imaging techniques for historical paintings - a review, Spectrochim. Acta Part B At. Spectrosc. 136 (2017) 81–105, https://doi.org/10.1016/j.sab.2017.08.003.
[11] S. Majumdar, J.R. Peralta-Videa, H. Castillo-Michel, J. Hong, C.M. Rico, J. L. Gardea-Torresdey, Applications of synchrotron μ-XRF to study the distribution of biologically important elements in different environmental matrices: a review, Anal. Chim. Acta 755 (2012) 1–16, https://doi.org/10.1016/j.aca.2012.09.050.
[12] I. Liritzis, N. Zacharias, Portable XRF of archaeological artifacts: current research, potentials and limitations, in: X-Ray Fluorescence Spectrometry (XRF) in Geoarchaeology, 2010, pp. 109–142.
[13] Y. Najman, The detrital record of orogenesis: a review of approaches and techniques used in the Himalayan sedimentary basins, Earth Sci. Rev. (2005), https://doi.org/10.1016/j.earscirev.2005.04.004.
[14] B.L. Drake, R.F. Shannon, Chapter 2. Principles of X-ray fluorescence, in: B. L. Drake, B.L. MacDonald (Eds.), Advances in Portable X-ray Fluorescence Spectrometry: Instrumentation, Application and Interpretation, Royal Society of Chemistry, 2022, pp. 11–50.
[15] M.J. Berger, et al., XCOM: photon cross sections database. https://www.nist.gov/pml/xcom-photon-cross-sections-database, 2009.
[16] R.E. Van Grieken, A.A. Markowicz (Eds.), Handbook of X-Ray Spectrometry, CRC Press, 2001.
[17] A.H. Compton, CXVII. The total reflexion of X-rays, London, Edinburgh Dublin Phil. Mag. J. Sci. 45 (270) (Jun. 1923) 1121–1131, https://doi.org/10.1080/14786442308634208.
[18] P.J. Potts, Portable X-ray Fluorescence Spectrometry : Capabilities for in Situ Analysis, Rsc Publishing, Cop PP - Cambridge, 2008.
[19] K. Tsuji, J. Injuk, R. Van Grieken (Eds.), X-Ray Spectrometry: Recent Technological Advances, John Wiley & Sons, 2005.
[20] R. Klockenkämper, A. Von Bohlen, Total-Reflection X-ray Fluorescence Analysis and Related Methods, Wiley PP - Hoboken, New Jersey, 2015.
[21] B. Kanngießer, W. Malzer, I. Reiche, A new 3D micro X-ray fluorescence analysis set-up – first archaeometric applications, Nucl. Instrum. Methods Phys. Res. Sect. B Beam Interact. Mater. Atoms 211 (2) (2003) 259–264, https://doi.org/10.1016/S0168-583X(03)01321-1.
[22] C. Vanhoof, J.R. Bacon, U.E.A. Fittschen, L. Vincze, Atomic spectrometry update: review of advances in X-ray fluorescence spectrometry and its special applications, J. Anal. At. Spectrom. 39 (9) (2024) 2152–2164, https://doi.org/10.1039/D4JA90034K.
[23] K. Shaker, et al., Longitudinal In-Vivo X-Ray fluorescence computed tomography with molybdenum nanoparticles, IEEE Trans. Med. Imag. 39 (12) (2020) 3910–3919, https://doi.org/10.1109/TMI.2020.3007165.
[24] G.M. Saladino, P.-H. Chao, B. Brodin, S.-D. Li, H.M. Hertz, Liposome biodistribution mapping with in vivo X-ray fluorescence imaging, Nanoscale 16 (37) (2024) 17404–17411, https://doi.org/10.1039/D4NR02793K.
[25] T.L. Sheppard, et al., In situ multimodal 3D chemical imaging of a hierarchically structured Core@Shell catalyst, J. Am. Chem. Soc. 139 (23) (Jun. 2017) 7855–7863, https://doi.org/10.1021/jacs.7b02177.
[26] S.K. Gill, et al., Quantitative nanoscale 3D imaging of intergranular corrosion of 304 stainless steel using hard X-Ray nanoprobe, J. Electrochem. Soc. 166 (11) (May 2019) C3320–C3325, https://doi.org/10.1149/2.0401911jes.
[27] E. Andresen, I.J. Flores-Sanchez, D. Brückner, S.N.H. Bokhari, G. Falkenberg, H. Küpper, Sublethal and lethal Cd toxicity in soybean roots specifically affects the metabolome, Cd binding to proteins and cellular distribution of Cd, J. Hazard Mater. 442 (September 2022) (Jan. 2023) 130062, https://doi.org/10.1016/j.jhazmat.2022.130062.
[28] C. Vanhoof, J.R. Bacon, A.T. Ellis, L. Vincze, P. Wobrauschek, Atomic spectrometry update – a review of advances in X-ray fluorescence spectrometry and its special applications,", J. Anal. At. Spectrom. 33 (9) (2018) 1413–1431, https://doi.org/10.1039/C8JA90030B, 2018.
[29] C. Vanhoof, J.R. Bacon, U.E.A. Fittschen, L. Vincze, Atomic spectrometry update: review of advances in X-ray fluorescence spectrometry and its special applications, J. Anal. At. Spectrom. 37 (9) (2022) 1761–1775, https://doi.org/10.1039/d2ja90035a.
[30] H. Rotella, et al., Elemental depth profiling in transparent conducting oxide thin film by X-ray reflectivity and grazing incidence X-ray fluorescence combined analysis, Spectrochim. Acta Part B At. Spectrosc. 135 (2017) 22–28, https://doi.org/10.1016/j.sab.2017.06.011.
[31] J. Baumann, et al., Laboratory setup for scanning-free grazing emission X-ray fluorescence, Anal. Chem. 89 (3) (Feb. 2017) 1965–1971, https://doi.org/10.1021/acs.analchem.6b04449.

[32] V. Szwedowski-Rammert, et al., Laboratory based GIXRF and GEXRF spectrometers for multilayer structure investigations, J. Anal. At. Spectrom. 34 (5) (2019) 922–929, https://doi.org/10.1039/C8JA00427G.
[33] W. Pessoa, et al., Grazing incident X-ray fluorescence combined with X-ray reflectometry metrology protocol of telluride-based films using in-lab and synchrotron instruments, Spectrochim. Acta Part B At. Spectrosc. 149 (June) (2018) 143–149, https://doi.org/10.1016/j.sab.2018.07.003.
[34] T. Sun, et al., Characterization of a confocal three-dimensional micro X-ray fluorescence facility based on polycapillary X-ray optics and Kirkpatrick-Baez mirrors, Spectrochim. Acta Part B At. Spectrosc. 63 (1) (2008) 76–80, https://doi.org/10.1016/j.sab.2007.11.003.
[35] L.J. Bauer, et al., Absorption correction for 3D elemental distributions of dental composite materials using laboratory confocal Micro-X-ray fluorescence spectroscopy, Anal. Chem. 96 (21) (2024) 8441–8449, https://doi.org/10.1021/acs.analchem.4c00116.
[36] J. Tapia, et al., Improving the characterization of red coloring matter from prehistoric cave art by means of laboratory confocal XRF depth profiling combined with synchrotron XRF imaging, J. Cult. Herit. 67 (2024) 385–394, https://doi.org/10.1016/j.culher.2024.03.018.
[37] J.F. Byrnes, P.J. Bush, Practical considerations in trace element analysis of bone by portable X-ray fluorescence, J. Forensic Sci. 61 (4) (Jul. 2016) 1041–1045, https://doi.org/10.1111/1556-4029.13103.
[38] S. Cagno, et al., Combined computed nanotomography and nanoscopic x-ray fluorescence imaging of cobalt nanoparticles in Caenorhabditis elegans, Anal. Chem. 89 (21) (2017) 11435–11442, https://doi.org/10.1021/acs.analchem.7b02554.
[39] S. Weber, et al., Multimodal hard X-ray nanotomography probes pore accessibility of technical catalysts after coking, ChemCatChem 16 (22) (Nov. 2024), https://doi.org/10.1002/cctc.202301298.
[40] B. Kanngießer, W. Malzer, I. Mantouvalou, D. Sokaras, A.G. Karydas, A deep view in cultural heritage—confocal micro X-ray spectroscopy for depth resolved elemental analysis, Appl. Phys. A 106 (2) (2011) 325–338, https://doi.org/10.1007/s00339-011-6698-0.
[41] R. Zito, L. Bonizzoni, N. Ludwig, Application of macro X-ray fluorescence fast mapping to thickness estimation of layered pigments, Sustainability 16 (6) (2024) 2467, https://doi.org/10.3390/su16062467.
[42] A. Dal Fovo, M. Morello, A. Mazzinghi, C. Toso, M. Galeotti, R. Fontana, Spectral mapping techniques for the stratigraphic and compositional characterisation of a 16th-Century painting, Heritage 7 (3) (2024) 1320–1333, https://doi.org/10.3390/heritage7030063.
[43] T. Cavaleri, et al., Tracing the history of past treatments: a multi-analytical study of a 16th-century panel painting copy after Raphael, J. Cult. Herit. 66 (2024) 142–154, https://doi.org/10.1016/j.culher.2023.11.010.
[44] J. Orsilli, S. Caglio, Combined scanned macro X-Ray fluorescence and reflectance spectroscopy mapping on corroded ancient bronzes, Minerals 14 (2) (2024) 192, https://doi.org/10.3390/min14020192.
[45] J. Dik, K. Janssens, G. Van Der Snickt, L. van der Loeff, K. Rickers, M. Cotte, Visualization of a lost painting by Vincent van gogh using synchrotron radiation based X-ray fluorescence elemental mapping, Anal. Chem. 80 (16) (2008) 6436–6442, https://doi.org/10.1021/ac800965g.
[46] M. Alfeld, J.A.C. Broekaert, Mobile depth profiling and sub-surface imaging techniques for historical paintings—A review, Spectrochim. Acta B Atom Spectrosc. 88 (2013) 211–230, https://doi.org/10.1016/j.sab.2013.07.009.
[47] K. Nakano, K. Tsuji, Nondestructive elemental depth profiling of Japanese lacquerware 'Tamamushi-nuri' by confocal 3D-XRF analysis in comparison with micro GE-XRF, X Ray Spectrom. 38 (5) (Sep. 2009) 446–450, https://doi.org/10.1002/xrs.1163.
[48] J. Orsilli, AR-XRF techniques for the analysis of cultural heritage layered samples. https://hdl.handle.net/10281/403656, 2022.
[49] J.-H. Liang, P.-P. Liu, Z. Chen, G.-X. Sun, H. Li, Rapid evaluation of arsenic contamination in paddy soils using field portable X-ray fluorescence spectrometry, J. Environ. Sci. 64 (2018) 345–351, https://doi.org/10.1016/j.jes.2017.11.020.
[50] R. Hennekam, T. Sweere, R. Tjallingii, G.J. de Lange, G.-J. Reichart, Trace metal analysis of sediment cores using a novel X-ray fluorescence core scanning method, Quat. Int. 514 (2019) 55–67, https://doi.org/10.1016/j.quaint.2018.10.018.
[51] M. Rincheval, D.R. Cohen, F.A. Hemmings, Biogeochemical mapping of metal contamination from mine tailings using field-portable XRF, Sci. Total Environ. 662 (2019) 404–413, https://doi.org/10.1016/j.scitotenv.2019.01.235.
[52] C. Porfido, et al., Correlations between as in earthworms' coelomic fluid and as bioavailability in highly polluted soils as revealed by combined laboratory X-ray techniques, Environ. Sci. Technol. 53 (18) (2019) 10961–10968, https://doi.org/10.1021/acs.est.9b02310.
[53] K. Nakano, C. Nishi, K. Otsuki, Y. Nishiwaki, K. Tsuji, Depth elemental imaging of forensic samples by confocal micro-XRF method, Anal. Chem. 83 (9) (2011) 3477–3483, https://doi.org/10.1021/ac1033177.
[54] K. Langstraat, et al., Large area imaging of forensic evidence with MA-XRF, Sci. Rep. 7 (1) (2017), https://doi.org/10.1038/s41598-017-15468-5.
[55] A. Knijnenberg, A. van Loon, J. Dik, A. van Asten, Elemental imaging of forensic traces with macro- and Micro-XRF, in: R.D. Blackledge (Ed.), Leading Edge Techniques in Forensic Trace Evidence Analysis, Wiley, 2022, pp. 213–244.
[56] S. Staeck, et al., Investigation of Ti nanostructures via laboratory scanning-free GEXRF, Nanoscale 17 (6) (2024) 3411–3420, https://doi.org/10.1039/d4nr02445a.
[57] K.B. Beć, C.W. Huck, Breakthrough potential in near-infrared spectroscopy: spectra simulation. A review of recent developments, Front. Chem. 7 (2019) 48.
[58] J. Workman Jr., L. Weyer, Practical Guide to Interpretive near-infrared Spectroscopy, CRC Press, 2007.
[59] C. Pasquini, Near infrared spectroscopy: fundamentals, practical aspects and analytical applications, J. Braz. Chem. Soc. 14 (2003) 198–219.
[60] V. Tuchin, Tissue Optics Light Scattering Methods and Instruments for Medial Diagnosis 13, SPIE, 2000, https://doi.org/10.1117/3.684093.
[61] C.S. Rajapakse, M. V Padalkar, H.J. Yang, M. Ispiryan, N. Pleshko, Non-destructive NIR spectral imaging assessment of bone water: comparison to MRI measurements, Bone 103 (2017) 116–124.
[62] R. Ailavajhala, J. Oswald, C.S. Rajapakse, N. Pleshko, Environmentally-controlled near infrared spectroscopic imaging of bone water, Sci. Rep. 9 (1) (2019) 10199.
[63] H. Cen, Y. He, Theory and application of near infrared reflectance spectroscopy in determination of food quality, Trends Food Sci. Technol. 18 (2) (2007) 72–83, https://doi.org/10.1016/j.tifs.2006.09.003.
[64] M. Manley, Near-infrared spectroscopy and hyperspectral imaging: non-destructive analysis of biological materials, Chem. Soc. Rev. 43 (24) (2014) 8200–8214.
[65] S. Jacques, Optical properties of biological tissues: a review, Phys. Med. Biol. 58 (2013) R37–R61, https://doi.org/10.1088/0031-9155/58/11/R37.
[66] D.G. Fraser, R.B. Jordan, R. Künnemeyer, V.A. McGlone, Light distribution inside mandarin fruit during internal quality assessment by NIR spectroscopy, Postharvest Biol. Technol. 27 (2) (2003) 185–196, https://doi.org/10.1016/S0925-5214(02)00058-3.
[67] A. Rodríguez-Ortega, N. Aleixos, J. Blasco, F. Albert, S. Munera, Study of light penetration depth of a Vis-NIR hyperspectral imaging system for the assessment of fruit quality. A case study in persimmon fruit, J. Food Eng. 358 (2023) 111673.
[68] M. V Padalkar, N. Pleshko, Wavelength-dependent penetration depth of near infrared radiation into cartilage, Analyst 140 (7) (2015) 2093–2100.
[69] J. Lammertyn, A. Peirs, J. De Baerdemaeker, B. Nicolaï, Light penetration properties of NIR radiation in fruit with respect to nondestructive quality assessment, Postharvest Biol. Technol. 18 (2) (2000) 121–132, https://doi.org/10.1016/S09255214(99)00071X.
[70] M. Huang, et al., Penetration depth measurement of near-infrared hyperspectral imaging light for milk powder, Sensors 16 (4) (2016) 441.
[71] I.O. Afara, et al., Characterization of connective tissues using nearinfrared spectroscopy and imaging, Nat. Protoc. 16 (2) (2021) 1297–1329, https://doi.org/10.1038/s4159602000468z.
[72] W.F. Cheong, S.A. Prahl, A.J. Welch, A review of the optical properties of biological tissues, IEEE J. Quant. Electron. 26 (12) (1990) 2166–2185, https://doi.org/10.1109/3.64354.
[73] X. Cui, S. Bray, A.L. Reiss, Functional near infrared spectroscopy (NIRS) signal improvement based on negative correlation between oxygenated and deoxygenated hemoglobin dynamics, Neuroimage 49 (4) (2010) 3039–3046.
[74] W.-L. Chen, et al., Functional near-infrared spectroscopy and its clinical application in the field of neuroscience: advances and future directions, Front. Neurosci. 14 (2020) 724.
[75] F. Faris, et al., Non-invasive in vivo near-infrared optical measurement of the penetration depth in the neonatal head, Clin. Phys. Physiol. Meas. 12 (4) (1991) 353, https://doi.org/10.1088/0143-0815/12/4/005.
[76] D. Huang, et al., Optical coherence tomography, Science 254 (5035) (1991) 1178–1181, https://doi.org/10.1126/science.1957169.
[77] J.G. Fujimoto, C. Pitris, S.A. Boppart, M.E. Brezinski, Optical coherence tomography: an emerging technology for biomedical imaging and optical biopsy, Neoplasia 2 (1) (2000) 9–25, https://doi.org/10.1038/sj.neo.7900071.
[78] P. Targowski, M. Iwanicka, Optical coherence tomography: its role in the noninvasive structural examination and conservation of cultural heritage objects—a review, Appl. Phys. A 106 (2) (2012) 265–277, https://doi.org/10.1007/s0033901166873.
[79] O. Berntsson, T. Burger, S. Folestad, L.-G. Danielsson, J. Kuhn, J. Fricke, Effective sample size in diffuse reflectance Near-IR spectrometry, Anal. Chem. 71 (3) (1999) 617–623, https://doi.org/10.1021/ac980652u.
[80] O.Y. Rodionova, et al., NIR spectrometry for counterfeit drug detection: a feasibility study, Anal. Chim. Acta 549 (1) (2005) 151–158, https://doi.org/10.1016/j.aca.2005.06.018.
[81] J. Burger, A. Gowen, Data handling in hyperspectral image analysis, Chemometr. Intell. Lab. Syst. 108 (1) (2011) 13–22, https://doi.org/10.1016/j.chemolab.2011.04.001.
[82] L.O. Svaasand, R. Ellingsen, Optical properties of human brain, Photochem. Photobiol. 38 (3) (1983) 293–299.
[83] F.B. Haeussinger, S. Heinzel, T. Hahn, M. Schecklmann, A.-C. Ehlis, A. J. Fallgatter, Simulation of near-infrared light absorption considering individual head and prefrontal cortex anatomy: implications for optical neuroimaging, PLoS One 6 (10) (2011) e26377.
[84] S. Perrey, Non-invasive NIR spectroscopy of human brain function during exercise, Methods 45 (4) (2008) 289–299, https://doi.org/10.1016/j.ymeth.2008.04.005.
[85] J. Yadav, A. Rani, V. Singh, B.M. Murari, Prospects and limitations of non-invasive blood glucose monitoring using near-infrared spectroscopy, Biomed. Signal Process Control 18 (2015) 214–227, https://doi.org/10.1016/j.bspc.2015.01.005.
[86] F.C. Clarke, S. V Hammond, R.D. Jee, A.C. Moffat, Determination of the information depth and sample size for the analysis of pharmaceutical materials using reflectance near-infrared microscopy, Appl. Spectrosc. 56 (11) (2002) 1475–1483.

[87] J.M.A. Mauritz, R.S. Morrisby, R.S. Hutton, C.H. Legge, C.F. Kaminski, Imaging pharmaceutical tablets with optical coherence tomography, J. Pharmaceut. Sci. 99 (1) (2010) 385–391.
[88] C.S.C. Yang, et al., Comprehensive study of solid pharmaceutical tablets in visible, near infrared (NIR), and longwave infrared (LWIR) spectral regions using a rapid simultaneous ultraviolet/visible/NIR (UVN) + LWIR laser-induced breakdown spectroscopy linear arrays detection, Opt. Express 25 (22) (2017) 26885–26897, https://doi.org/10.1364/OE.25.026885.
[89] E. Botonjic-Sehic, M. Tsaparikos, C. Brown, M. Lamontagne, Forensic Application of near-infrared Spectroscopy: Aging of Bloodstains, 2009.
[90] M.A. de Carvalho, et al., NIR hyperspectral images for identification of gunshot residue from tagged ammunition, Anal. Methods 10 (38) (2018) 4711–4717.
[91] M. Longoni, B. Genova, A. Marzanni, D. Melfi, C. Beccaria, S. Bruni, FT-NIR spectroscopy for the non-invasive study of binders and multi-layered structures in ancient paintings: Artworks of the Lombard Renaissance as case studies, Sensors 22 (5) (2022), https://doi.org/10.3390/s22052052.
[92] C. Cucci, J.K. Delaney, M. Picollo, Reflectance hyperspectral imaging for investigation of works of art: old master paintings and illuminated manuscripts, Acc. Chem. Res. 49 (10) (2016) 2070–2079, https://doi.org/10.1021/acs.accounts.6b00048.
[93] E. Catelli, et al., Towards the non-destructive analysis of multilayered samples: a novel XRF-VNIR-SWIR hyperspectral imaging system combined with multiblock data processing, Anal. Chim. Acta 1239 (2023) 340710, https://doi.org/10.1016/j.aca.2022.340710.
[94] M. Vega-Castellote, M.-T. Sánchez, J.P. Wold, N.K. Afseth, D. Pérez-Marín, Near infrared light penetration in watermelon related to internal quality evaluation, Postharvest Biol. Technol. 204 (2023) 112477.
[95] C. V Greensill, K.B. Walsh, A remote acceptance probe and illumination configuration for spectral assessment of internal attributes of intact fruit, Meas. Sci. Technol. 11 (12) (2000) 1674.
[96] A. Laborde, et al., A partial least squares-based approach to assess the light penetration depth in wheat flour by near infrared hyperspectral imaging, J. Near Infrared Spectrosc. 28 (1) (2020) 25–36.
[97] M. Almeida, K.E. Torrance, A.K. Datta, Measurement of optical properties of foods in Near- and mid-infrared radiation, Int. J. Food Prop. 9 (4) (2006) 651–664, https://doi.org/10.1080/10942910600853667.
[98] M. Dagerskog, L. Osterstrom, INFRA-RED RADIATION FOR FOOD PROCESSING. I: A STUDY OF THE FUNDAMENTAL PROPERTIES OF INFRA-RED RADIATION, 1979.
[99] R.E. Thilwind, G.W. t'Hooft, N. Uzunbajakava, Improved depth resolution in near-infrared diffuse reflectance spectroscopy using obliquely oriented fibers, J. Biomed. Opt. 14 (2) (2009) 24026, https://doi.org/10.1117/1.3103339.
[100] A. Gianoncelli, G. Kourousias, Limitations of portable XRF implementations in evaluating depth information: an archaeometric perspective, Appl. Phys. A 89 (2007) 857–863.
[101] L. Musílek, T. Trojek, R. Prokeš, Techniques for identifying depth inhomogeneities of elemental distribution in materials, Radiat. Phys. Chem. 167 (2020) 108344.
[102] T. Trojek, L. Musílek, R. Prokeš, Depth of layers in historical materials measurable by X-ray fluorescence analysis, Radiat. Phys. Chem. 155 (2019) 239–243.

Supplementary Information

Exploiting the penetration depth of NIR and XRF radiation: from 2D to 3D spectral imaging

Zelan Li[1], Carolina Scagliarini[2], Alberto Mazzoleni[2], Sara Gariglio[3,4], Emilio Catelli[1], Cristina Malegori[3], Silvia Prati[1], Eugenio Alladio[2,*], Giorgia Sciutto[1,*], Paolo Oliveri[3,*]

[1]*Department of Chemistry "Giacomo Ciamician", University of Bologna, Via Guaccimanni 42, 48121 Ravenna, Italy*

[2]*Department of Chemistry, University of Turin, Via Pietro Giuria 7, Torino, Italy*

[3]*Department of Pharmacy (DIFAR), University of Genova, Viale Cembrano 4, Genova, Italy*

[4]*Department of Chemistry and Industrial Chemistry (DCCI), University of Genova, Via Dodecaneso 31, Genova, Italy*

**Corresponding Authors: eugenio.alladio@unito.it, giorgia.sciutto@unibo.it, paolo.oliveri@unige.it*

Table S1: Queries used for conducting searches in the Scopus database to analyse publication trends and subject areas of XRF spectroscopy

XRF spectroscopy	TITLE-ABS-KEY(("XRF" OR "x-ray W/1 fluorescence" OR "x-ray W/1 fluorescent"))
XRF imaging	TITLE-ABS-KEY(("XRF" OR "x-ray W/1 fluorescence" OR "x-ray W/1 fluorescent") AND ("imaging" W/3 "xrf" OR "mapping" W/3 "xrf" OR "scanning" W/3 "xrf"))
XRF penetration depth	• TITLE-ABS-KEY (xrf AND penetration) OR TITLE-ABS-KEY (xrf AND depth) • TITLE-ABS-KEY(("XRF" OR "x-ray W/1 fluorescence" OR "x-ray W/1 fluorescent")AND ((penetration W/5 depth) OR "information depth" OR "sampling depth" OR "depth profile" OR "depth profiling" OR "depth-resolved" OR "stratigraphy" OR "stratigraphic"))

Table S2: Queries used for conducting searches in the Scopus database to analyse publication trends and subject areas of NIR spectroscopy

NIR spectroscopy	TITLE-ABS-KEY (("NIR" OR "near W/1 infrared" OR "near-infrared") AND (spectroscop*))
NIR penetration depth	TITLE-ABS-KEY (("NIR" OR "near W/1 infrared" OR "near-infrared") AND (spectroscop*)) AND ((penetration W/5 depth) OR "information depth" OR "sampling depth" OR "depth profile" OR "depth profiling" OR "depth-resolved" OR "stratigraphy" OR "stratigraphic")